https://doi.org/10.5194/egusphere-2026-2020
Preprint. Discussion started: 21 April 2026

Enhanced Water Mass Mixing in Fram Strait in 2020 and elevated Circulation Timescales of Atlantic-derived Waters in 2021 based on Transient Tracers I-129 and U-236

Marcel Scheiwiller[1], Anne-Marie Wefing[2], Habacuc Pérez-Tribouillier[1,3], Christof Vockenhuber[1,3], Paul A. Dodd[2], Justin P. Gwynn[4], and Núria Casacuberta[1,3]

[1]Department of Environmental Systems Science, ETHZ, Zürich, Switzerland
[2]Norwegian Polar Institute, Tromsø, Norway
[3]Laboratory of Ion Beam Physics, Department of Physics, ETHZ, Zürich, Switzerland
[4]Norwegian Radiation and Nuclear Safety Authority, Tromsø, Norway

Correspondence: Marcel Scheiwiller (marcel.scheiwiller@usys.ethz.ch) and Núria Casacuberta (nuria.casacubertaarola@usys.ethz.ch)

Abstract.

The world's oceans are responding to anthropogenically induced climate change, with the Arctic Ocean being identified as one of the most rapidly changing regions. Quantifying the circulation and mixing timescales of Atlantic-origin waters in the Fram Strait—the primary gateway for Arctic-Atlantic exchange—is essential for understanding the evolving connectivity between the Arctic and the subpolar North Atlantic. This study utilizes the anthropogenic radionuclide tracer pair, Iodine-129 (^{129}I) and Uranium-236 (^{236}U), to investigate the origin and transit history of water masses sampled between 2016 and 2021. By applying a consistent methodological framework using both binary mixing and Transit Time Distribution (TTD) models to surface Polar Water and mid-depth Arctic Atlantic Water, we assess the temporal stability of the regional circulation regime. Our results reveal significant interannual variability. Waters outflowing the Fram Strait in 2020 exhibited a higher degree of mixing and a stronger influence from Amerasian Basin sourced waters compared to 2016 and 2021. We identify a distinct water parcel on the Greenland Shelf with a tracer signature indicating a long-path circulation from the Canada Basin in 2020. Finally, we find a tendency towards elevated circulation timescales in 2021 that are related to either slower circulation timescales or longer circulation pathways. These findings highlight the importance of further assessing the temporal evolution of Atlantic Waters arriving in Fram Strait as the Atlantic layer brings heat to the Arctic Ocean.

1 Introduction

1.1 Fram Strait – The Primary Gateway Between the Arctic Ocean and the Subpolar North Atlantic

The Fram Strait serves as the principal gateway for water mass exchange between the Arctic Ocean and the subpolar North Atlantic. On its eastern side, the West Spitsbergen Current (WSC) (Fig. 1) transports relatively warm and saline Atlantic Water into the Eurasian Basin (Aagaard and Reed, 1987; Timmermans and Marshall, 2020), acting as a major heat source for the Arc-

https://doi.org/10.5194/egusphere-2026-2020
Preprint. Discussion started: 21 April 2026

tic Ocean (Schauer et al., 2004; Besczynska-Möller et al., 2011; Smedsrud et al., 2022), continuously gaining relevance as the Atlantic Water temperatures are increasing (Wang et al., 2020). This process has received increasing attention due to Atlantification — the progressive intrusion of increasingly warm Atlantic Water into the Arctic Ocean, a process also observed in the Fram Strait itself (Tesi et al., 2021) — which is now observed to extend beyond the Eurasian Basin into the Amerasian Basin (Ingvaldsen et al., 2021; Polyakov et al., 2023, 2025b). The enhanced presence of Atlantic Water weakens vertical stratification, promotes upward heat flux, and accelerates sea ice melt, contributing to Arctic Ocean Amplification, whereby temperatures rise more than two times faster than the global average (Previdi et al., 2021; Shu et al., 2022). These unprecedented changes driven by anthropogenic climate change are projected to result in a seasonally ice-free Arctic Ocean by mid-century (Box et al., 2019; Kim et al., 2023; Jahn et al., 2024), with significant implications for circulation dynamics (Meredith et al., 2019).

On the western side of the strait, the East Greenland Current (EGC) transports water masses from the central Arctic Ocean to the subpolar North Atlantic (Aagaard and Reed, 1987) with its core situated at the Greenland shelf slope (Rudels et al., 2002). The EGC reflects the integrated outcome of upstream Arctic circulation and is composed of two primary layers in the upper part: a surface layer of cold, low-salinity Polar Water and a mid-depth layer of relatively warmer and saltier Arctic Atlantic Water (Woodgate, 2013). These layers play a critical role in modulating freshwater and heat fluxes to the North Atlantic (Bras et al., 2021) and the freshwater flux has shown to vary temporally (Karpouzoglou et al., 2022, 2024). The Arctic Ocean is an important player in contributing waters to the Atlantic Meridional Overturning Circulation (AMOC) (Weijer et al., 2022; Zhang and Thomas, 2021; Dey et al., 2024) and therefore ultimately influencing stratification and deep water formation of the AMOC's lower limb.

The upper layer of the EGC, the surface Polar Water, typically occupies the top $250\ \mathrm{m}$, is characterized by potential densities (σ_0) below 27.7 kg m^{-3} and includes the polar mixed layer and the halocline (Rudels, 2009, 2021). Polar Water comprises a mixture of Pacific Water entering through the Bering Strait (orange arrows in Fig.1) and Atlantic Water entering via the Barents Sea Opening (green arrows in Fig.1). The Atlantic component, entering as the Norwegian Coastal Current (NCC), follows a coastal path through the Barents Sea and into the Nansen Basin, eventually reaching the Fram Strait via the Transpolar Drift (Rudels and Carmack, 2022; Pérez-Tribouillier et al., 2025). Along this route, surface waters are modified by freshwater inputs from Siberian rivers and sea-ice melt, resulting in dilution and enhanced stratification (Fichot et al., 2013). The Pacific component enters through Bering Strait, becoming part of the Beaufort Gyre and ultimately joining the Transpolar Drift towards Fram Strait (Rudels, 2021; Rudels and Carmack, 2022). The fraction of Pacific Water in Polar Water outflowing Fram Strait is of great interest to improve predictions of freshwater export from the Arctic Ocean to the subpolar North Atlantic as the Pacific Water is relatively fresh compared to Atlantic Water and contributes substantially to the freshwater budget (Rabe et al., 2013; Carmack et al., 2016). The Pacific Water fraction has traditionally been estimated using nutrient-based tracers (Jones et al., 1998, 2003; Falck et al., 2005, 2008; Dodd et al., 2012), with the composition in the Fram Strait varying substantially over time (Falck et al., 2008; Dodd et al., 2012) and showing a dependence on the Arctic Ocean index (Steele et al., 2004). However, these nutrient-based tracers do not act in the conservative way as previously assumed (Alkire et al., 2019, 2015; Bauch et al.,

https://doi.org/10.5194/egusphere-2026-2020
Preprint. Discussion started: 21 April 2026

2011). Modeling efforts rendered minor fractions of Pacific Water, which needs to be validated by observations (Lique et al., 2010). The recent exploration of the new Gallium tracer has shown to deliver promising results to disentangle Atlantic and Pacific contributions (Whitmore et al., 2020; McAlister and Orians, 2015). However, there is a need for further research and the exploration of alternatives as a state of the art tracer is still missing. Using Iodine-129 (^{129}I) and Uranium-236 (^{236}U) as a new tracer tool to disentangle Pacific and Atlantic contributions has shown to be another promising approach that will be used here again in a qualitative way (Wefing et al., 2022).

The Arctic Atlantic Water layer, typically residing between 400 m and 700 m depth (Rudels, 2009), is a blend of Atlantic Water flowing through the Arctic Ocean via two main pathways: a long route through the Canada and Makarov Basins (Woodgate et al., 2001; Karcher et al., 2012; Smith et al., 1999), and a shorter route through the Amundsen and Nansen Basins (purple arrows in Fig.1) (Woodgate et al., 2001; Aksenov et al., 2011; Rudels et al., 2015; Wefing et al., 2019). Compared to Polar Water, Arctic Atlantic Water is characterized by a density range of $\sigma_0 \approx 27.7$ to 27.97 kg m^{-3} (Rudels, 2009, 2021) and consists of two main branches: Fram Strait Branch Water (FSBW), which entered via the Fram Strait, and Barents Sea Branch Water (BSBW), which entered via the Barents Sea. Both branches converge in the St. Anna Trough and form the Arctic Ocean Boundary Current circulating cyclonically along the continental slope (Smith et al., 2011; Rudels et al., 2015, 1994). These relatively warm branches are of considerable scientific interest, primarily due to their increasing potential to transfer heat upward, and thereby act as a positive feedback loop of accelerating sea ice melting (Wang et al., 2024; Polyakov et al., 2020a). Consequently, quantifying and assessing the variability of circulation timescales and pathways for Arctic Atlantic Water is paramount not only for understanding the influence of this heat-bearing layer on the Arctic climate system in its recent past and future (Polyakov et al., 2023; Årthun et al., 2026; Brown et al., 2025) but also for comprehending its ecological impact (Greene et al., 2008).

Apart from the described outflowing layers Polar Water and Arctic Atlantic Water, the Fram Strait is a two-way gateway, facilitating also inflowing water masses within the WSC, which makes it a region of intense mixing. A portion of the WSC recirculates within the strait and merges with the EGC, forming Recirculating Atlantic Water (Quadfasel et al., 1987; Hattermann et al., 2016; Rudels, 2021). Approximately half of the Atlantic Water entering the strait between 76° N and 81° N is estimated to recirculate as Recirculating Atlantic Water (Marnela et al., 2013; de Steur et al., 2014), with a southern and northern recirculation at around 78.5° N and 80° N (black arrows in Fig.1b) (Hofmann et al., 2021). This process is partly driven by mesoscale eddies that can extend westward into the EGC (Hattermann et al., 2016). The Recirculating Atlantic Water subducts beneath the Polar Water as it joins the EGC due to its greater density and mixes with the Arctic Atlantic Water at mid-depth (Marnela et al., 2013; Hattermann et al., 2016; Appen et al., 2016; Hofmann et al., 2021). Efforts to understand the recirculation in the Fram Strait have mostly gone into describing the existence, magnitude, location, and seasonality of recirculation (Quadfasel et al., 1987; Manley, 1995; Marnela et al., 2013; Appen et al., 2016; Hattermann et al., 2016; Wekerle et al., 2017; Hofmann et al., 2021). However, temporal dynamics of the recirculation regime are still not well understood but have implications on the melt rate on the Northeast Greenland shelf (McPherson et al., 2023). Here we study the origin of the water masses in the Fram

https://doi.org/10.5194/egusphere-2026-2020
Preprint. Discussion started: 21 April 2026

Strait in different years, which brings further light into temporal recirculation processes.

Given its role as the primary outflow pathway, the western Fram Strait offers a valuable observational window into upstream Arctic processes and their integrated effects. Both Polar Water and Arctic Atlantic Water are central to the transmission of Arctic changes to the subpolar North Atlantic. Advancing our understanding of the circulation timescales, mixing and provenance of these water masses is therefore essential for assessing the evolving dynamics of the Arctic–Atlantic system. To this end, we employ the transient radionuclide tracers ^{129}I and ^{236}U, which provide powerful constraints on the circulation timescales of Arctic–Atlantic waters.

https://doi.org/10.5194/egusphere-2026-2020
Preprint. Discussion started: 21 April 2026

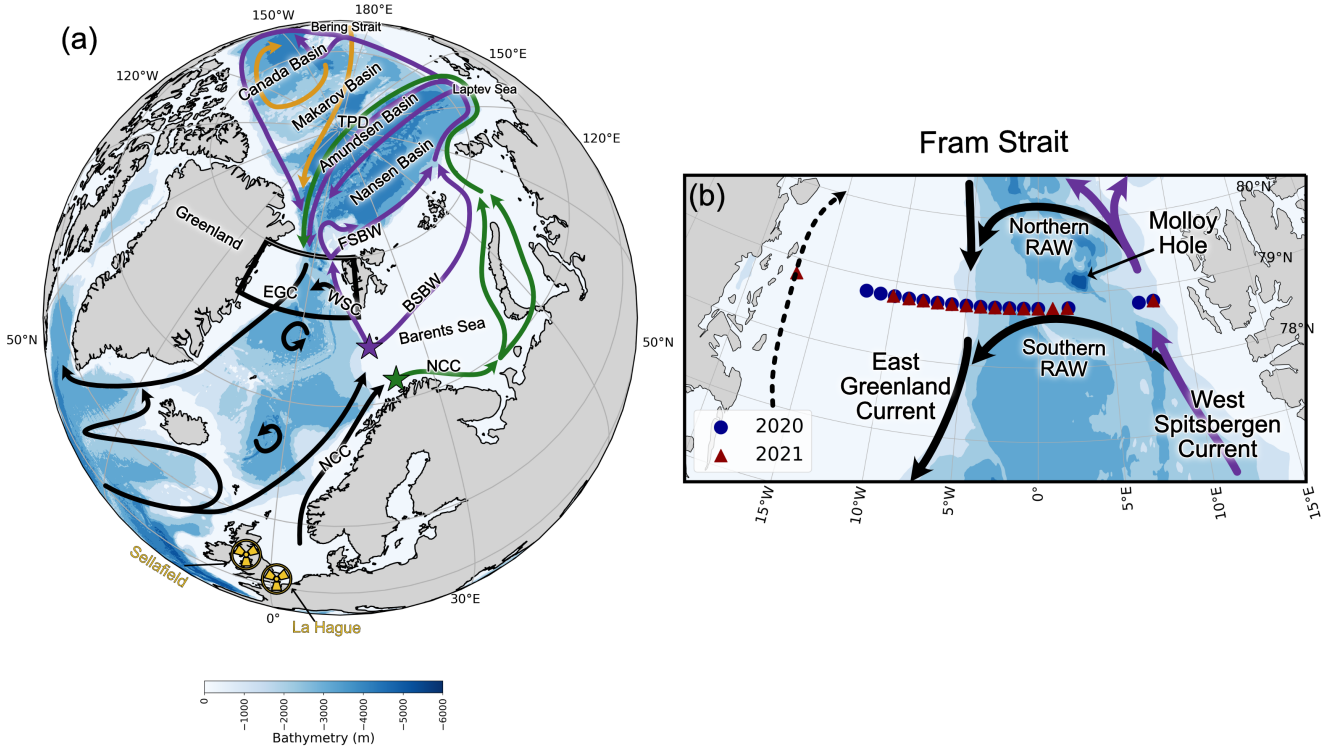

Figure 1. (a) Overview map of the main circulation regime in the Arctic and North Atlantic. The location of the Nuclear Reprocessing Plants is shown as yellow radioactive symbols. The location of the two radionuclide input functions are indicated as green (surface layer) and purple (mid-depth layer) stars (the input functions are shown in Fig. 2). The surface Atlantic-derived circulation regime is indicated as green arrows with orange arrows showing the Pacific influence from Bering Strait. The mid-depth circulation regime is shown as purple arrows. Inlet (b) depicts a more detailed circulation regime in the Fram Strait, showing the stations sampled during 2020 and 2021 for the purpose of this work.

1.2 Anthropogenic Radionuclides ^{129}I and ^{236}U as Tracers of Circulation Timescales and Mixing in the Fram Strait

The anthropogenic radioisotopes ^{129}I and ^{236}U serve as tracers for assessing the dynamics of the Arctic-Atlantic system and quantifying circulation timescales in the Fram Strait (Wefing et al., 2019, 2021, 2022). While initially focused on the Fram Strait, applications have recently expanded to the central Arctic Ocean, the Canadian Basin, the Iceland, Labrador, Barents, and Lincoln Seas (Payne et al., 2024; Leist et al., 2024; Dale et al., 2024; Pérez-Tribouillier et al., 2025; Wefing et al., 2025). Both isotopes are long-lived (half-lives: $^{129}\mathrm{I} = 15.7$ Ma; $^{236}\mathrm{U} = 23.4$ Ma) and behave conservatively in the open ocean (Edmonds

https://doi.org/10.5194/egusphere-2026-2020
Preprint. Discussion started: 21 April 2026

et al., 2001; Christl et al., 2012; Casacuberta et al., 2014).

Their presence in the marine environment arises from: (i) Nuclear Reprocessing Plants (NRPs), the primary source for both isotopes is liquid discharge from the Sellafield (UK) and La Hague (France) facilities (see Fig. 1); and (ii) global fallout, a secondary, substantial source for ^{236}U is global fallout from atmospheric nuclear weapons testing in the 1960s (Sakaguchi et al., 2009). This input is negligible for ^{129}I (Raisbeck et al., 1995; Snyder et al., 2010). The input functions for both tracers entering the Arctic Ocean have been defined (Casacuberta et al., 2018) and updated (Wefing et al., 2021) at the Barents Sea Opening (Fig. 1). Crucially, the signal timing differs: the major injection of ^{129}I occurred in the late 1990s, whereas the peak ^{236}U input occurred earlier, in the 1960s (Fig. 2).

Historically, various tracer-based approaches have been employed to estimate the circulation timescales of Atlantic-derived waters. Rudels et al. (2000) inferred a return pathway of FSBW of under 10 years based on temperature anomalies. Subsequently, multi-tracer studies using ^{129}I, Cesium-137 (^{137}Cs), and chlorofluorocarbon-11 (CFC-11) estimated ages of 8–10 years for surface layers and 9–15 years for mid-depth waters near the North Pole (Smith et al., 2011). Similarly, Stöven et al. (2016) applied a Transit Time Distribution (TTD) model using chlorofluorocarbon-12 (CFC-12) and sulfur hexafluoride (SF_6) in the Fram Strait, deriving mean ages of 7 ± 6 years for Polar Water and 32 ± 15 years for Arctic Atlantic Water. While effective for ventilation timescales, the application of gaseous tracers in surface layers is constrained by air-sea exchange, a process likely to intensify with diminishing sea ice (Bates et al., 2006). Conversely, radionuclides offer a robust alternative for investigating lateral circulation timescales (Wefing et al., 2021; Casacuberta and Smith, 2023; Raimondi et al., 2024; Payne et al., 2024).

The first ^{129}I transect in the Fram Strait was obtained in 2002 (Alfimov et al., 2004, 2013). At that time, the high-concentration signal from the 1990s had not yet transited the central Arctic Ocean; thus, the signal served primarily as an indicator of immediate Atlantic Water recirculation. More recently, Wefing et al. (2019) combined ^{129}I and ^{236}U to model circulation timescales, estimating 12–19 years for surface Polar Water and 16–23 years for mid-depth Arctic Atlantic Water based on binary mixing with radionuclide-free Pacific or fresh waters. Wefing et al. (2021) refined this using a TTD approach incorporating flow-field mixing (Haine and Hall, 2002), yielding updated ages of 5–18 years for Arctic Atlantic Water. Other combinations, such as ^{236}U with Colored Dissolved Organic Matter (CDOM), have yielded transit times of 7–27 years for the upper water column (Lin et al., 2023a).

Despite this progress, the Fram Strait circulation regime remains poorly constrained due to two main limitations. First, methodological inconsistency hinders direct comparison: previous studies have alternated between *tracer ages* (Wefing et al., 2019; Lin et al., 2023a; Körtke et al., 2024) and *TTDs* (Wefing et al., 2021; Stöven et al., 2016), yielding divergent results. Second, the temporal variability of these circulation timescales remains poorly constrained.

https://doi.org/10.5194/egusphere-2026-2020
Preprint. Discussion started: 21 April 2026

Motivated by these gaps, this study combines new ^{129}I data from 2020 and 2021 with ^{236}U data from Lin et al. (2023a) to address three specific objectives. We calculate tracer ages for the surface Polar Water layer (binary mixing model) and extend the TTD method to the surface layer. This establishes a uniform methodological framework, allowing for a direct comparison between surface and mid-depth layers. Then, we qualitatively delineate the proportional Amerasian water contribution in the Fram Strait surface layer from the Eurasian water using a mixing model and TTD results. Finally, we evaluate the temporal stability of the circulation regime by comparing the new 2020 and 2021 estimates with data from 2016 published in Wefing et al. (2019).

2 Materials and Methods

2.1 Sample Collection, Processing and Measurements

Water samples were collected during two oceanographic expeditions to the Fram Strait aboard the RV *Kronprins Haakon*, conducted from 24 August 2020 to 13 September 2020, and from 31 July 2021 to 20 August 2021. These expeditions were part of the annual monitoring program coordinated by the Norwegian Polar Institute (de Steur, 2021, 2022). A total of 119 samples for ^{129}I analysis were collected in 2020, and 115 in 2021. Concurrently, a separate research group collected samples for ^{236}U measurements published in Lin et al. (2023a). For intercomparison purposes and adding additional data in the WSC, we also processed a subset of our samples for ^{236}U measurements, amounting to 22 from 2020 and 11 from 2021. The results of this intercomparison are presented in Fig. A1 and demonstrate good agreement. Consequently, all ^{236}U concentrations used in this study refer to the dataset published by Lin et al. (2023a). Seawater was sampled using 12 L Niskin bottles mounted on a conductivity-temperature-depth (CTD) rosette. Samples were transferred into pre-rinsed 1 L plastic cubitainers and stored at the Norwegian Polar Institute in Tromsø following the expedition. The 2020 samples were processed at the Norwegian Polar Institute, while the 2021 samples were shipped to ETH Zurich for further analysis. Approximately 200 mL aliquots were used for ^{129}I processing, with the remaining volume allocated for ^{236}U measurements. A subset of the ^{129}I data from 2021 has been published in Pérez-Tribouillier et al. (2025). In addition to this data, we incorporated ^{129}I and ^{236}U concentrations from the Fram Strait in 2016 into our analysis (Wefing et al., 2019). The stations from 2016 are shown in Fig. A2 together with stations from 2020 and 2021.

After the expedition, ^{129}I samples were processed according to the method described in Casacuberta et al. (2016). The seawater samples (200 mL) were spiked with approximately 1.5 mg of Iodine-127 (^{127}I). Both Iodine isotopes were isolated from the seawater matrix and precipitated as silver iodide (AgI). The silver iodide powder was pressed into titanium holders and inserted into the 500 kV *Tandy* Accelerator Mass Spectrometry (AMS) system at the Laboratory of Ion Beam Physics at ETH Zurich to measure the ratio of ^{129}I/^{127}I (Vockenhuber et al., 2015). The known spiked amount of the stable isotope ^{127}I was then used to derive the ^{129}I concentration. An in-house standard, C2, with known concentrations of 5.055×10^{-12} at at^{-1} ^{129}I/^{127}I (diluted) and 38.995×10^{-12} at at^{-1} ^{129}I/^{127}I (concentrated) was measured alongside the samples. The relative dif-

https://doi.org/10.5194/egusphere-2026-2020
Preprint. Discussion started: 21 April 2026

ference between the measured C2 concentrations to the nominal value was used to normalize the value of the samples. MilliQ water blanks (18.2 MΩ high-purity water) from the laboratory were used to correct for the background level of ^{129}I. They were included in every processing run, amounting to 21 blanks and 7 blanks for the samples from 2020 and 2021, respectively. Additionally, an expedition-specific internal standard was included for repeat measurements of the same sample, which resulted in a 4 % uncertainty. For further details on the processing and the measurements, we refer to Casacuberta et al. (2016); Payne et al. (2024).

In total 33 ^{236}U samples were processed according to the method of Christl et al. (2015) and compared to Lin et al. (2023a) (see Fig. A1). The seawater samples (1 L) were spiked with approximately 1 pg of Uranium-233 (^{233}U). Uranium isotopes were concentrated with Fe co-precipitation and isolated from the seawater matrix with ion exchange chromatography (UTEVA resin columns). Uranium was oxidized and pressed into targets for measurements with the 300 kV *MILEA* AMS system at the Laboratory of Ion Beam Physics at ETH Zurich. The ratios of ^{233}U/^{238}U and ^{236}U/^{238}U were measured and the known amount of spiked ^{233}U was then used to derive the ^{236}U concentration. An in-house standard, ZUTRI, was measured alongside to normalize the samples with known ratios of $(33,170 \pm 830) \times 10^{-12}$ at at^{-1} for ^{233}U/^{238}U, and $(4,055 \pm 200) \times 10^{-12}$ at at^{-1} for ^{236}U/^{238}U. MilliQ water blanks (18.2 MΩ high-purity water) from the laboratory were used to correct for the background level of ^{236}U. They were included in every processing run, amounting to 3 blanks in total. For further details on the processing and the measurements, we refer to Christl et al. (2015, 2023) and Payne et al. (2024).

2.2 Water Mass Classification in the Fram Strait

To characterize the seawater samples according to their hydrographic properties, we use the classification scheme of Rudels (2021). Based on that, we defined 7 different water masses, which are listed in Table 1. Polar Water I and Polar Water I warm include the Pacific-derived water, the Polar Mixed Layer, shelf water, and the upper halocline. Polar Water I warm is further subcategorized due to seasonal summer heating and ice melt contribution (Rudels et al., 2000). Polar Water II consists of the Atlantic-derived lower halocline and the winter mixed layer from the Nansen Basin and Barents Sea. Atlantic Water is part of the WSC, arriving from the North Atlantic Ocean. The Recirculating Atlantic Water originates from the WSC (same properties as Atlantic Water) but has left the core of the WSC. The Arctic Atlantic Water is also of Atlantic origin, but has already circulated through the Arctic Ocean and so it has changed its properties. Finally, we broadly categorize samples in deeper layers below the Arctic Atlantic Water into Intermediate and Deep Waters. As these layers are not the main objective of this study, we refrain from assigning more detailed categories. Samples that did not meet the defined boundaries were labeled as a mixture of two water masses based on their hydrographic profile.

Samples categorized as Polar Water I were used to estimate circulation timescales with two models: (i) the binary mixing model (section 2.3.2) and (ii) the TTD model (section 2.3.4). For Arctic Atlantic Water samples only the TTD model (section 2.3.3) was used to estimate circulation timescales. Both models rely on an input function that defines the concentrations

https://doi.org/10.5194/egusphere-2026-2020
Preprint. Discussion started: 21 April 2026

of ^{129}I and ^{236}U entering the Arctic Ocean in a given year.

Table 1. Categorization of samples into water masses according to the definition of Rudels (2021).

# in 2016	# in 2020	# in 2021	Water Mass	Pot. Density (kg m^{-3})	Pot. Temp. (°C)
19	51	40	Polar Water I	$\sigma_0 \leq 27.20$	$\theta \leq 0$
2	5	8	Polar Water I Warm	$\sigma_0 \leq 27.20$	$0 < \theta$
9	14	19	Polar Water II	$27.20 < \sigma_0 \leq 27.70$	$\theta \leq 0$
22	14	9	Atlantic Water	$27.70 < \sigma_0 \leq 27.97$	$2 < \theta^a$
13	18	14	Recirculating Atlantic Water	$27.70 < \sigma_0 \leq 27.97$	$2 < \theta^a$
28	8	20	Arctic Atlantic Water	$27.70 < \sigma_0 \leq 27.97$	$0 < \theta \leq 2$
39	1	6	Intermediate & Deep Waters	$27.97 < \sigma_0$	-

[a]Samples were divided into Atlantic Water and Recirculating Atlantic Water based on the geographical location, whereas Atlantic Water samples were at either 7° E or 8° E, and Recirculating Atlantic Water samples were further to the west.

2.3 Estimation of Circulation Timescales and Mixing

2.3.1 Input Function of ^{129}I and ^{236}U into the Arctic Ocean

To characterize the time-dependent input of the radionuclide tracers ^{129}I and ^{236}U into the Arctic Ocean, two input functions were defined (Fig. 2a,b): (i) the Atlantic Layer input function, located at 74° N and 19° E, and (ii) the NCC input function, located at 71° N and 22° E (Wefing et al., 2021). Their geographical positions are illustrated in Fig. 1, both located at the Barents Sea opening (Casacuberta et al., 2018; Wefing et al., 2021). These input functions serve as the upstream boundary conditions for estimating circulation timescales and mixing processes at downstream locations, such as the Fram Strait.

We distinguish between surface and mid-depth input functions, as they correspond to different water masses with distinct tracer concentrations (Casacuberta et al., 2018). The surface input function reflects the propagation of the NCC, while the mid-depth input function represents the continuation of the Atlantic Layer, which includes both the FSBW and the BSBW. These branches originate from Atlantic Water that undergoes progressive cooling and densification as it advects through the Fram Strait and Barents Sea, respectively (Rudels and Carmack, 2022). Upon reaching the Nansen Basin near the St. Anna Trough, the BSBW subducts beneath the FSBW due to its longer cooling trajectory. As the combined flow continues eastward along the Siberian continental slope, enhanced isopycnal mixing gradually homogenizes the vertical structure, forming a unified mid-depth layer (Rudels and Carmack, 2022).

Based on the water mass classification described in section 2.2, Polar Water I samples are considered to originate from the surface input function and are part of the Polar Mixed Layer. Polar Water II samples, which include the lower halocline, represent a transitional layer between Polar Water I and Arctic Atlantic Water. These samples may exhibit partial influence from

https://doi.org/10.5194/egusphere-2026-2020
Preprint. Discussion started: 21 April 2026

deeper Arctic Atlantic Water tracer signals. Furthermore, a uniform correction factor is applied to surface samples to account for the dilution with the low tracer signal from global fallout waters (see section 2.3.4). However, this factor may vary slightly with depth within the Polar Water II layer. For this reason, Polar Water II samples are excluded from the core analysis of surface and mid-depth layers. The Arctic Atlantic Water samples are interpreted as a downstream continuation of the mid-depth input function, encompassing both FSBW and BSBW components (Wefing et al., 2021). For a detailed description of the input function construction, we refer to Wefing et al. (2021).

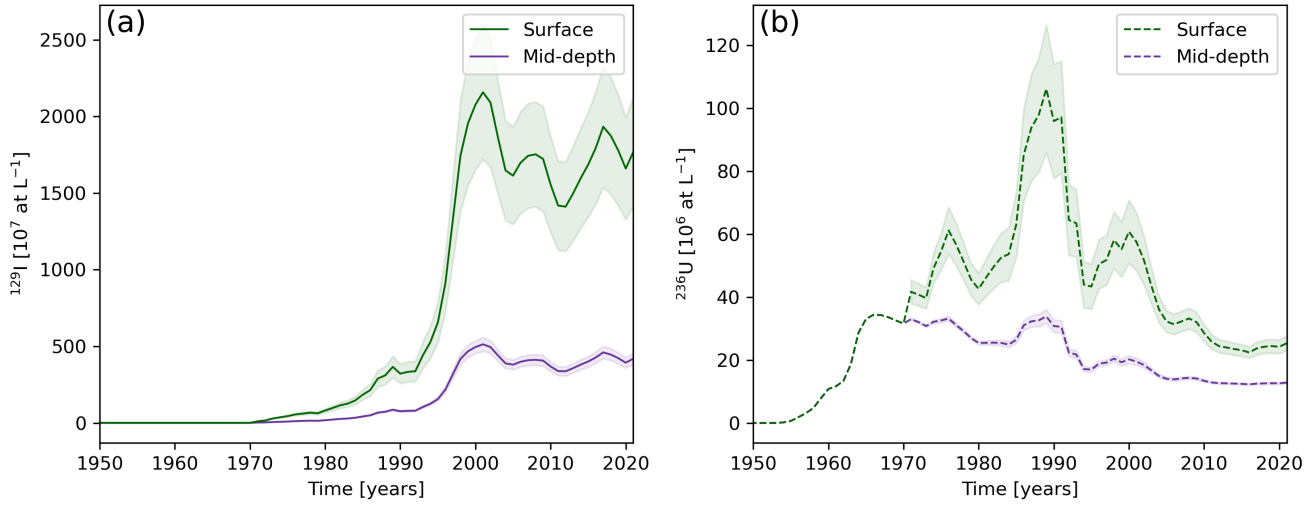

Figure 2. Input functions for ^{129}I (a) and ^{236}U (b) at the entrance of the Arctic Ocean for the Polar Water layer at the surface (green lines) and the Arctic Atlantic Water layer at mid-depth (purple lines) with uncertainties shown as shaded areas.

2.3.2 The Binary Mixing Model

Tracer ages for surface Polar Water I samples collected in 2016, 2020, and 2021 were estimated using a binary mixing model, following the methodology described by Wefing et al. (2021) and Payne et al. (2024). The model assumes mixing between two endmembers: (i) the time-dependent surface input functions of ^{129}I and ^{236}U, driven by the NRPs input to the ocean surface, and (ii) a background concentration of these tracers carried by Pacific and Atlantic waters that have not been in contact with the NRPs signal (see Fig. 1). The background levels were estimated to be 1.16×10^7 at L^{-1} for ^{129}I and 6.25×10^6 at L^{-1} for ^{236}U (Snyder et al., 2010; Chamizo et al., 2022; Dale et al., 2024). These are updated estimates of the background levels than previously used in Wefing et al. (2019). Therefore, the tracer ages were recalculated for the published 2016 dataset to be consistent when comparing the three years (2016, 2020, and 2021) used in this study. Sea ice meltwater and river water has been observed to carry low concentrations of ^{129}I and ^{236}U (Casacuberta et al., 2016, 2018). As these sources are not explicitly represented in the binary mixing model, tracer concentrations of all samples were corrected to a reference salinity of 34.8 to account for dilution effects associated with freshwater inputs. The reference salinity of 34.8 was calculated as the mean salinity

https://doi.org/10.5194/egusphere-2026-2020
Preprint. Discussion started: 21 April 2026

in the Arctic Ocean (Aagaard, 1989) and has since often been used as a reference (e.g., Karpouzoglou et al., 2022; Haine et al., 2023; Timmermans and Toole, 2023).

The salinity corrected concentration c_{sal} is calculated in the following:

$$c_{sal} = \frac{c_{init} \times Sal_{ref}}{Sal_{sample}} \tag{1}$$

where c_{init} is the initial measured concentration, Sal_{sample} is the salinity of each individual sample, and Sal_{ref} is the reference salinity 34.8.

The binary mixing model is illustrated in Fig. 3a, where each line represents the mixing trajectory between the background concentration and the input function for a specific year. The line closest to a given sample indicates the best-fit input year, thereby defining the tracer age of that sample as the difference between sampling year and input year. An example is shown in Fig. 3a that plots closest to the mixing line from 2000 and therefore corresponds to a tracer age of 16 years (assuming the example was sampled in 2016). The binary mixing model grid with the data from 2016, 2020, and 2021 plotted on top is shown in Fig. A3. Throughout this study, the term "tracer age" refers specifically to estimates derived from the binary mixing model, while "circulation timescale" is used more broadly to encompass age estimates from all applied methods. The uncertainty of tracer ages was assessed by calculating the minimum and maximum age estimates based on measurement uncertainties for both ^{129}I and ^{236}U.

The binary mixing model assumes purely advective transport and does not account for mixing between water parcels entering the Arctic Ocean in different years, which carry temporally variable tracer signals. While the surface layer is known to exhibit strong advective characteristics (e.g., Smith et al., 2011), this simplification represents a limitation of the binary mixing approach.

https://doi.org/10.5194/egusphere-2026-2020
Preprint. Discussion started: 21 April 2026

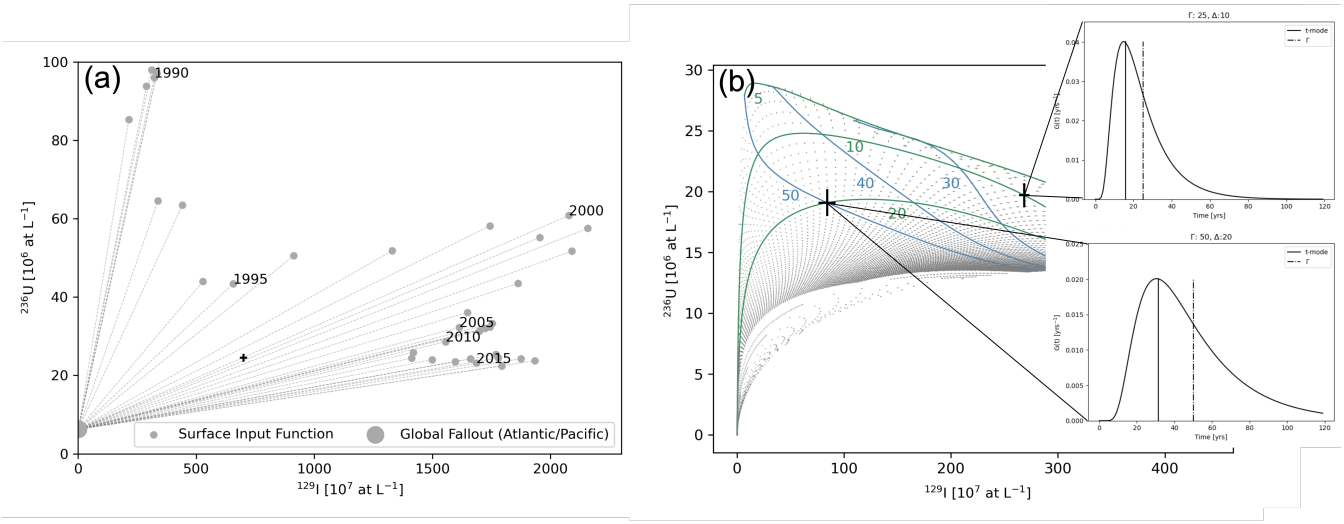

Figure 3. (a) The binary mixing model grid with a constant global fallout background level (large gray point) and a time varying input of ^{129}I and ^{236}U to the surface Arctic Ocean (small gray points). An example datapoint with its uncertainty is shown in black. (b) The TTD model grid of ^{129}I and ^{236}U concentrations. Each gray dot represents a possible Gamma (Γ)-Delta (Δ) combination based on the mid-depth input function with the uncertainties as gray lines. Isolines show the distribution of Γ's (blue lines) and Δ's (green lines). Two example datapoints are plotted on top of the grid (black). The insets show the probability density functions of these two examples.

2.3.3 The Transit Time Distribution Model at Mid-Depth

To address this limitation, the TTD model is applied as a complementary method. The TTD model provides a framework for estimating oceanic transport timescales and mixing processes by accounting for multiple pathways contributing to a given sampling location (Haine and Hall, 2002; Hall and Haine, 2002; Waugh et al., 2004). Although the mathematical formulation is one-dimensional, the model effectively incorporates the convergence of multiple water mass branches, making it particularly suitable for complex regions like the Arctic Ocean.

The TTD model, originally adapted to the oceanographic case by Haine and Hall (2002), has since been adopted in Arctic tracer studies (e.g., Smith et al., 2011, 2022; Wefing et al., 2021). Following the approach described in Wefing et al. (2021), we applied the TTD model to mid-depth Arctic Atlantic Water samples. We use the so-called "Smith's TTD approach" (Raimondi et al., 2024), which leverages the transient input of ^{129}I and ^{236}U into the Arctic Ocean (see section 2.3.1) to derive both the age spectrum and degree of mixing for each sample. A brief overview of the model is provided here; for further methodological details, see Wefing et al. (2021) and Raimondi et al. (2024).

The tracer concentration at a given location x and time t is given as:

https://doi.org/10.5194/egusphere-2026-2020
Preprint. Discussion started: 21 April 2026

$$c(x,t) = \int_0^\infty c_0(t-t')G(x,t')\,dt' \tag{2}$$

Here, $c_0(t)$ represents the time-dependent input function, and $G(t')$ is the Green's function, which describes the probability distribution of transit times. The Green's function is modeled as an inverse Gaussian distribution, capturing both advective and diffusive transport components in the ocean (Haine and Hall, 2002). It is interpreted as the probability that a water parcel originating at the source arrives at the sampling location after a time t (Haine et al., 2025):

$$G(x,t) = \sqrt{\frac{\Gamma^3}{4\pi\Delta^2 t^3}} exp(-\frac{\Gamma(t-\Gamma)^2}{4\Delta^2 t}) \tag{3}$$

The shape of the distribution is governed by two parameters: Γ, the mean transit time (mean age), and Δ, which characterizes the width of the distribution and thus the degree of mixing. A third parameter, the mode age t_{mode}, represents the most probable transit time and is calculated as:

$$t_{mode} = \frac{1}{\Gamma}(\sqrt{9\Delta^4 + \Gamma^4} - 3\Delta^2) \tag{4}$$

This parameter has been suggested as a more representative measure of lateral transport than the mean age (Smith et al., 2011; Wefing et al., 2021).

In practice, we assumed a range of possible Δ and Γ values (1–2000 years) and constrained their ratio Δ/Γ to lie between 0.1 and 1.8, following Raimondi et al. (2024). This resulted in a grid of possible ^{129}I and ^{236}U concentrations (Fig. 3b), where each grid point corresponds to a specific Γ–Δ pair. Sample concentrations were then mapped onto this grid, and the closest match determines the best-fit parameters for each sample. Two examples with the corresponding probability density functions are shown in Fig. 3b.

To estimate uncertainties, we performed a Monte Carlo simulation with 100 iterations. This included propagated uncertainties from tracer measurements. Additionally, uncertainties in the input function were incorporated into the simulation. These are visualized in Fig. 3b as uncertainty bars for the data points and as uncertainty envelopes around the grid points.

The TTD parameters in Arctic Atlantic Water were recalculated for the published 2016 dataset in Wefing et al. (2021) to be consistent when comparing the three years (2016, 2020, and 2021) used in this study. This resulted in slight differences to the published dataset due to updated background concentrations of the tracers. The grids with the data plotted on top are shown in Fig. A4 for all years.

https://doi.org/10.5194/egusphere-2026-2020
Preprint. Discussion started: 21 April 2026

2.3.4 The Transit Time Distribution Model at the Surface

In addition to applying the TTD model to mid-depth Arctic Atlantic Water, for the first time here, we extended its use to surface Polar Water I samples. This novel application enables direct comparison of transit times across vertical layers in the Fram Strait and provides a more accurate representation of mixing processes along surface pathways.

Surface waters in the Fram Strait are influenced by a complex mixture of Atlantic Water, Pacific Water, shelf water, and sea ice meltwater. Shelf water, sea ice meltwater and the Atlantic/Pacific component that carry the global fallout tracer signal all dilute the Atlantic Water signal that carries the NRPs signal. To account for these effects, we applied two corrections to the measured ^{129}I and ^{236}U concentrations. First, we corrected for freshwater dilution by normalizing tracer concentrations to the reference salinity of 34.8 (Aagaard, 1989), consistent with the correction applied in the binary mixing model (Eq. 1). Second, we accounted for the tracer-free global fallout contribution by subtracting the background tracer levels. Identical to the binary mixing model, the background concentrations of 1.16×10^7 at L^{-1} for ^{129}I and 6.25×10^6 at L^{-1} for ^{236}U were used (Snyder et al., 2010; Chamizo et al., 2022).

The corrected tracer concentrations (c_{corr}) were calculated using the following formula:

$$c_{corr} = \frac{c_{sal} - c_{GF} \times f_{GF}}{f_{Atl}} \tag{5}$$

where c_{sal} is the salinity corrected concentration (Eq. 1), c_{GF} is the global fallout concentration, and f_{GF} and f_{Atl} are the fractional contributions of global fallout water of Pacific and (old) Atlantic origin and the Atlantic Water branch carrying the tracer signals, respectively, with $f_{GF} = 1 - f_{Atl}$.

Both the f_{GF} and f_{Atl} from Eq. 5 are not well-known. We assume that the global fallout contribution (f_{GF}) in surface waters is entirely of Pacific origin. In the past, nutrient based analysis by Dodd et al. (2012) reported a Pacific Water fraction range of 40 % to 80 %. In this work, we tested different fractions within this range and the proportion that best fit our data was 55 % (see Fig. A5, illustrating the TTD grid obtained with corrections of 45 %, 55 %, and 65 %). Additionally, we explored an alternative correction method using nutrient-based estimates of Pacific Water fractions for each individual sample. However, this approach produced unrealistic tracer concentrations that fell outside the defined TTD model grid, and was therefore not used in the final analysis.

For all years (2016, 2020, 2021), TTD parameters in Polar Water I were calculated as part of this study. The grids with the data plotted on top are shown in Fig. A4.

https://doi.org/10.5194/egusphere-2026-2020
Preprint. Discussion started: 21 April 2026

3 Results

3.1 Distributions of ^{129}I in the Fram Strait in 2020 and 2021

^{129}I concentrations are represented as depth profiles in Fig. 4, grouped into five main regions along the section (detailed results are on Zenodo: Scheiwiller (2026)). Two general ^{129}I concentration patterns emerged in 2020 and 2021. First, ^{129}I concentrations generally decreased with depth across the entire study area. Notable exceptions to this trend were observed at stations from the Greenland Shelf region, where increases towards the bottom were detected at certain stations in 2020. Second, overall higher ^{129}I concentrations were observed in the 2021 sampling campaign compared to the 2020 campaign across most regions.

https://doi.org/10.5194/egusphere-2026-2020
Preprint. Discussion started: 21 April 2026

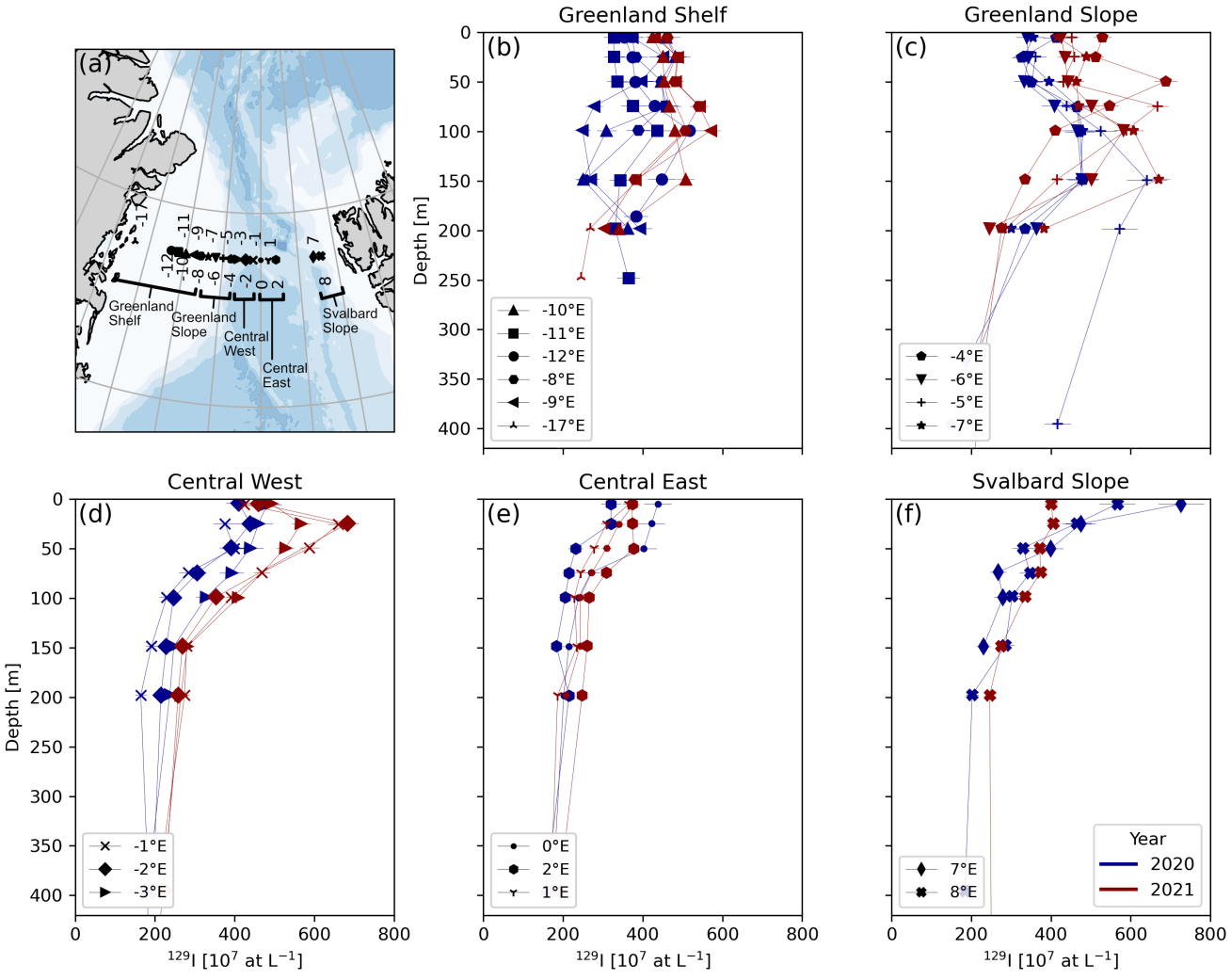

Figure 4. Depth profiles of ^{129}I concentrations in 2020 (blue) and 2021 (red). The stations are divided into five regions (indicated on the map in panel a): Greenland Shelf (b, -17° E to -7° E), Greenland Slope (c, -6° E to -4° E), Central West (d, -3° E to -1° E), Central East (e, 0° E to 3° E), and Svalbard Slope (f, 7° E/8° E).

The "Greenland Shelf" region extended from -17° E to -8° E with five stations in 2020 and four stations in 2021 (Fig. 4b). Stations -11° E and -12° E were only sampled in 2020, while station -17° E was only sampled in 2021. For the entire shelf region ^{129}I concentrations ranged from (248 ± 20) to $(517 \pm 41) \times 10^7$ at L^{-1} in 2020 (depths 5–200 m) and from (303 ± 13) to $(571 \pm 24) \times 10^7$ at L^{-1} in 2021 (depths 5–200 m). In both years, concentrations were relatively constant in the upper 50 m. In 2021, concentrations increased to a maximum around 100 m depth, and decreased towards greater depths. In 2020, we observed two different patterns. Stations -8° E and -12° E followed a similar trend as stations in 2021. However, at stations -9° E, -10° E, and less pronounced at station -11° E, we observed a minimum in concentrations around 75–150 m depth, and then

https://doi.org/10.5194/egusphere-2026-2020
Preprint. Discussion started: 21 April 2026

an increase again towards the bottom samples. These low ^{129}I concentrations between 75 and 150 m depth coincided with high ^{236}U concentrations reported by Lin et al. (2023a).

The "Greenland Slope" region between -4° E and -7° E was in the core southward flowing EGC and comprised the same four stations in 2020 and 2021 (Fig. 4c). ^{129}I concentrations ranged from (150 ± 12) to $(641 \pm 50) \times 10^7$ at L^{-1} in 2020 (depths 5–400 m) and from (177 ± 7) to $(688 \pm 29) \times 10^7$ at L^{-1} in 2021 (depths 5–1000 m). In both years, we observed elevated concentrations below the surface (between 50 and 200 m) and then decreasing to the seafloor. These elevated concentrations were at a deeper depth in 2020 (100–200 m) compared to 2021 (50–100 m).

The "Central West" region spanned from -3° E to -1° E, with three stations in 2020 and the same in 2021 (Fig. 4d). Concentrations for ^{129}I ranged from (15 ± 2) to $(481 \pm 38) \times 10^7$ at L^{-1} in 2020 (depths 5–2500 m) and from (173 ± 10) to $(683 \pm 29) \times 10^7$ at L^{-1} in 2021 (depths 5–1000 m) . The overall lowest concentration was observed in 2020 at 2500 m depth (-1° E), amounting to $(15 \pm 2) \times 10^7$ at L^{-1} (not shown in Fig. 4d). In 2021, all stations in this region showed a sub-surface peak at around 25 m and overall higher concentrations between 25–200 m compared to 2020, whereas concentrations in surface samples (5 m depth) were similar in both years.

The "Central East" part spanned from 0° E to 3° E with two stations in 2020 and three stations in 2021 (Fig. 4e). Concentrations for ^{129}I ranged from (157 ± 12) to $(438 \pm 34) \times 10^7$ at L^{-1} in 2020 (depths 5–400 m) and from (169 ± 7) to $(376 \pm 16) \times 10^7$ at L^{-1} in 2021 (depths 5–400 m). Station 2° E was generally lower in ^{129}I concentrations in 2020 compared to 2021, whereas station 0° E showed higher concentrations in the upper 50 m in 2020 compared to 2021.

The samples from the "Svalbard Slope" region were located in the WSC, transporting Atlantic Water into the Arctic Ocean (Fig. 4f). The region comprised two stations in 2020 (7° E and 8° E), and one station in 2021 (8° E). ^{129}I concentrations ranged from (184 ± 15) to $(727 \pm 57) \times 10^7$ at L^{-1} in 2020 (depths 5–400 m) and (21 ± 1) to $(405 \pm 17) \times 10^7$ at L^{-1} in 2021 (depths 5–1000 m). The highest concentrations were found at the surface, higher in 2020 compared to 2021.

3.2 ^{129}I Concentrations in the Context of Water Masses in 2020 and 2021

TS-diagrams with color-coded ^{129}I concentrations as well as section plots of ^{129}I concentrations relate the tracer distribution to water masses in the Fram Strait in 2020 (Fig. 5a,b) and 2021 (Fig. 5c,d). The samples collected in 2020 generally showed elevated ^{129}I concentrations in the the water masses Polar Water I and Atlantic Water (Fig. 5a). Lowest ^{129}I concentrations were found in Intermediate and Deep Waters. A subset of samples fell outside the Rudels (2021) classification, located between the 27.2 kg m^{-3} and 27.7 kg m^{-3} σ_0 isopycnals and with conservative temperatures above 0° C. These were classified as mixtures of Recirculating Atlantic Water and outflowing water masses such as Polar Water I, Polar Water II, or Polar Water I warm (see Table 1). The water masses from the TS diagram are also shown in the cross-section of ^{129}I (Fig. 5b). On the eastern side,

https://doi.org/10.5194/egusphere-2026-2020
Preprint. Discussion started: 21 April 2026

Atlantic Water occupied the water column along the Svalbard Slope, representing northward-flowing water entering the Arctic Ocean via the WSC. In the central region, Recirculating Atlantic Water dominated between 50–200 m depth. In the western Fram Strait, where the EGC dominates, Polar Water I and Polar Water II extended from the surface to $\sim$200 m depth, underlain by Arctic Atlantic Water reaching depths of $\sim$1,000 m. Beneath this, Intermediate and Deep Waters were present.

https://doi.org/10.5194/egusphere-2026-2020
Preprint. Discussion started: 21 April 2026

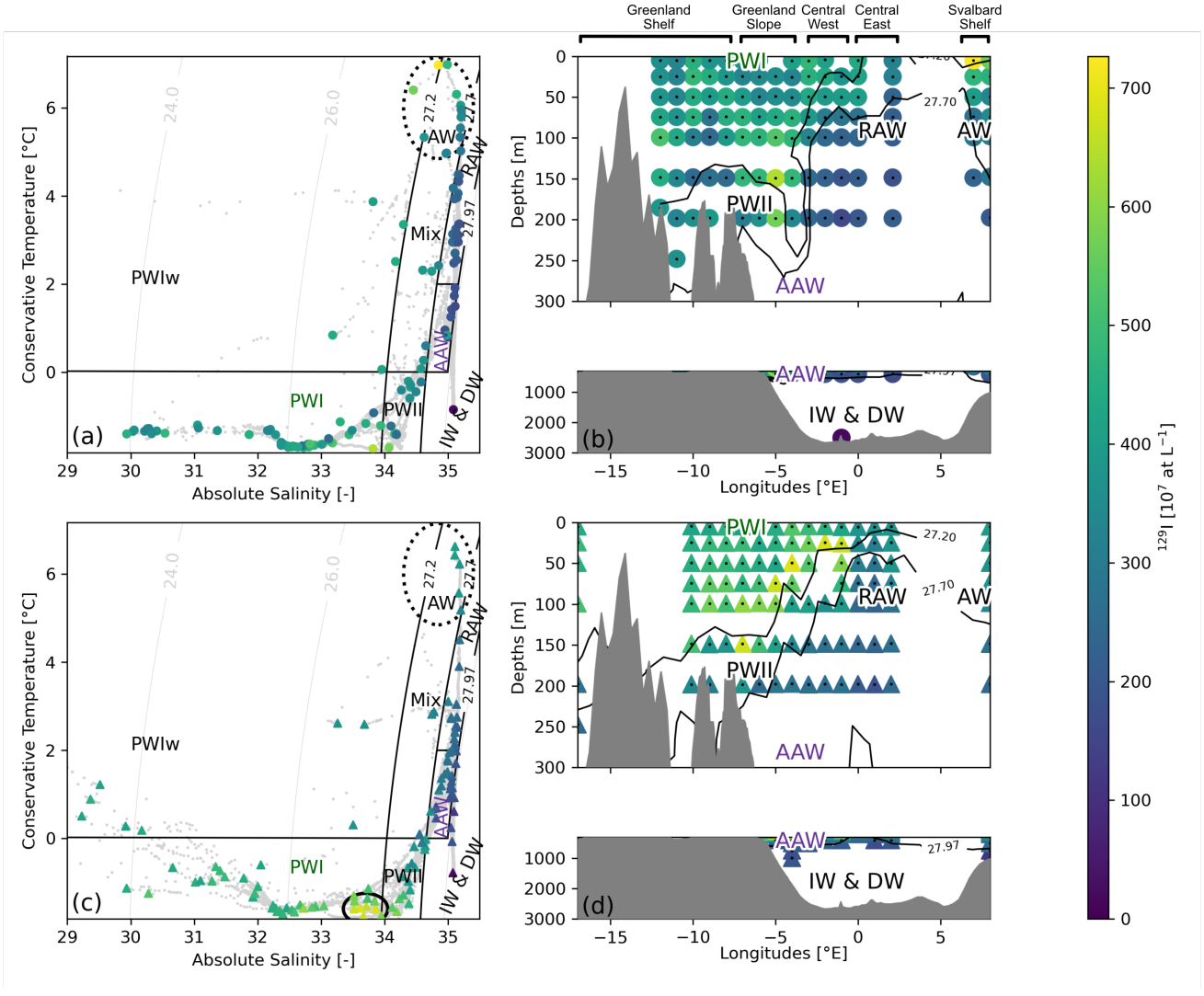

Figure 5. TS-diagrams and section plots of ^{129}I in 2020 (top, a and b) and 2021 (bottom, c and d). Panels a and c show Conservative Temperature vs. Absolute Salinity (TS-diagrams) with σ_0 isopycnals in light gray. Fram Strait 2020 (a) and 2021 (c) samples are plotted in the TS space as gray dots and with ^{129}I concentrations as a color-code where available. The category boundaries from Rudels (2021) (Table 1) are drawn as black lines whereas the dotted ellipse indicates Atlantic Water samples that are part of the WSC. The black ellipse highlights elevated ^{129}I concentrations. Panels b and c show cross-sections from the Greenland Shelf to Svalbard (-17° E to 8° E) at 78.9° N with color-coded ^{129}I concentrations from 2020 (b) and 2021 (d). Selected σ_0 isopycnals (black) are overlaid. Water mass acronyms in panels a to d correspond to the water masses defined in Table 1.

In 2021, the ^{129}I concentrations showed overall a similar distribution in TS space and in the cross-sectional view as in 2020 (Fig. 5c,d). However, a distinct cluster of elevated ^{129}I concentrations was observed within Polar Water I near the Polar Water II boundary in 2021 (black ellipse in Fig. 5c). In the central region in 2021, Recirculating Atlantic Water also dominated between

https://doi.org/10.5194/egusphere-2026-2020
Preprint. Discussion started: 21 April 2026

50–200 m depth, yet with Arctic Atlantic Water also being present, reaching unexpectedly shallow depths (∼75 m), despite typically residing between 400–700 m (Rudels, 2009).

The elevated ^{129}I concentrations observed in Polar Water I and Atlantic Water in the TS diagram in both years are also evident in the sectional view. The elevated ^{129}I concentrations in Polar Water I adjacent to Polar Water II appeared as a horizontal band between ∼50–200 m depth, most clearly in 2021. Surface samples in the central region included Polar Water I warm and mixed water masses, reflecting the dynamic mixing zone where inflowing and outflowing waters converge. This mixing front was particularly evident in 2020, characterized by a near-vertical σ_0 structure. Comparing both years, the position and orientation of the water mass front between inflow and outflow differed. In 2020, the front was more vertically aligned, with the 27.2 kg m^{-3} σ_0 isopycnal extending straight down near -3° E. In contrast, 2021 showed a more sloped front, with Polar Water I/Polar Water II reaching 0° E at the surface and gradually shifting westwards with depth. These differences were also reflected in the ^{129}I concentrations (Fig. 5b,d).

3.3 Tracer Ages of Surface Waters

Tracer age estimates for Polar Water I were derived from the binary mixing model (section 2.3.2) for the years 2016, 2020, and 2021 and are presented here as depth profiles, separated into three different regions (Fig. 6). The mean tracer age was 18 ± 1 in 2016, 22 ± 2 years in 2020, and 23 ± 1 years in 2021.

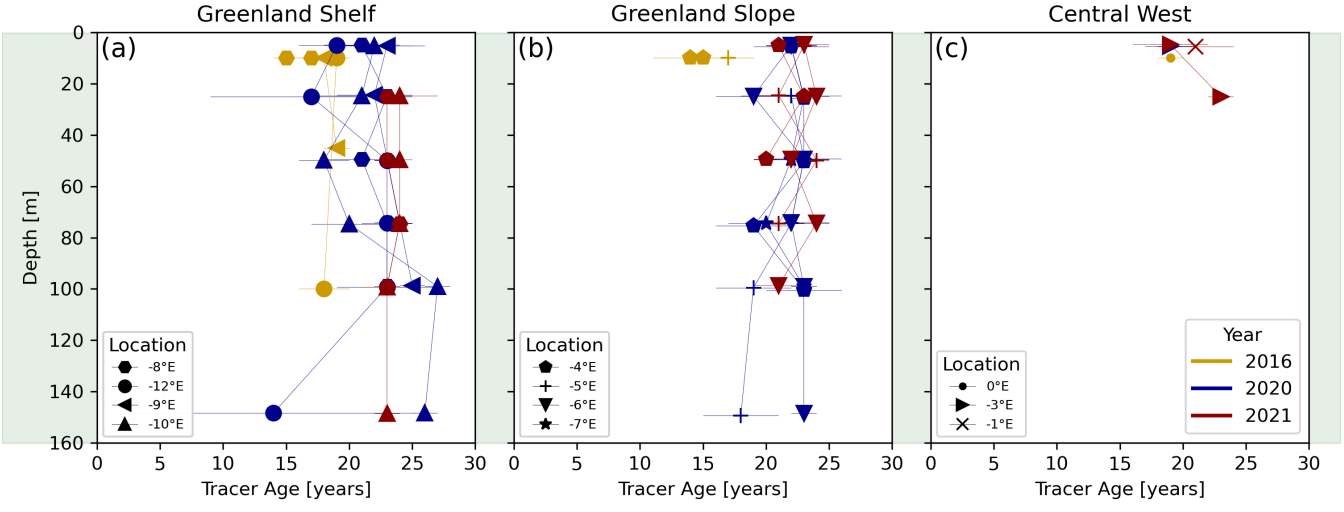

Figure 6. Tracer age results for Polar Water I at the surface (indicated by the green background color), divided in the three regions of the Greenland Shelf (a), the Greenland Slope (b), and Central West (c). Tracer ages are shown for the years 2016 (yellow), 2020 (blue), and 2021 (red).

https://doi.org/10.5194/egusphere-2026-2020
Preprint. Discussion started: 21 April 2026

In the Greenland Shelf region (Fig. 6a), tracer ages were almost constant over the entire depth range in 2016 and 2021, but showed a higher variability in 2020, encompassing both the overall lowest and highest tracer age. The youngest tracer age, 14 ± 12 years, was recorded at station -12° E at 150 m depth. Low tracer ages were also found at shallower depths at stations -10° E and -12° E. Elevated tracer ages were observed at station -9° E at 100 m depth (25 ± 1 years), and at station -10° E at both 150 m and 100 m depths (26 ± 1 and 27 ± 1 years, respectively). These samples were characterized by low ^{129}I concentrations (see section 3.1) and high ^{236}U concentrations. Regarding temporal trends, tracer ages in the upper 50 m showed an overall increase from 2016 to 2021.

In the Greenland Slope region (Fig. 6b), no temporal trends were observed between 2020 and 2021, since tracer ages were quite narrowly distributed over the entire depth range in both years, largely between 20 and 25 years. Data from 2016 was only available for two samples at 10 m depth, which showed a lower tracer age compared to the same station and depth in 2020 and 2021. In the Central West region (Fig. 6c), the few available Polar Water I samples had tracer ages around 20 years.

3.4 Circulation Timescales and mixing of Surface and Mid-depth Waters

Estimates of the TTD parameters t_{mode}, Γ, and Δ for 2016, 2020 and 2021 are shown as depth profiles in Fig. 7, calculated as described in sections 2.3.3 and 2.3.4, including samples from Arctic Atlantic Water and Polar Water I.

3.4.1 Mid-depth Arctic Atlantic Water

The mid-depth Arctic Atlantic Water layer showed t_{mode} ages ranging from 5 to 21 years in 2016 (mean: 14 ± 4 years), 7 to 25 years in 2020 (mean: 13 ± 7 years), and 9 to 24 years in 2021 (mean: 17 ± 6 years). Mean ages (Γ) spanned 18 to 57 years in 2016 (mean: 30 ± 10 years), 20 to 94 years in 2020 (mean: 54 ± 26 years) and 19 to 32 years in 2021 (mean: 27 ± 4 years). Mixing parameter (Δ) varied from 4 to 80 years in 2016 (mean: 18 ± 16 years), from 2 to 140 years in 2020 (mean: 56 ± 50 years), and from 5 to 16 years in 2021 (mean: 11 ± 4 years).

Due to the limited number of mid-depth samples in 2020 (n=7) and 2021 (n=9), spatial interpretation is constrained, but a general increase of all TTD parameters with depth was observed. The Greenland Slope — associated with the core of the EGC — exhibited the most homogeneous t_{mode}, Γ, and Δ distributions (Fig. 7b, e, h), consistent with reduced influence from other water masses. Notably, samples from the Central West region in 2020 showed lower t_{mode} ages (7–9 years, Fig. 7c) and elevated Δ values (51–140 years, Fig. 7i) compared to the Greenland Slope, likely indicating the presence of younger inflowing waters transported by the WSC and returning through Fram Strait (see section 4.2).

https://doi.org/10.5194/egusphere-2026-2020
Preprint. Discussion started: 21 April 2026

3.4.2 Surface Polar Water I

In surface Polar Water I, t_{mode} ages ranged from 2 to 15 years in 2016 (mean: 9 ± 3 years), from 3 to 28 years in 2020 (mean: 10 ± 5 years), and from 5 to 18 years in 2021 (mean: 12 ± 3 years). Mean ages (Γ) varied from 13 to 37 in 2016 (mean: 19 ± 6 years), from 15 to 96 years in 2020 (mean: 40 ± 18 years) and from 19 to 37 years in 2021 (mean: 25 ± 4 years). The mixing parameter (Δ) ranged from 4 to 36 in 2016 (mean: 11 ± 8 years), from 3 to 160 years in 2020 (mean: 41 ± 41 years) and from 4 to 34 years in 2021 (mean: 14 ± 7 years).

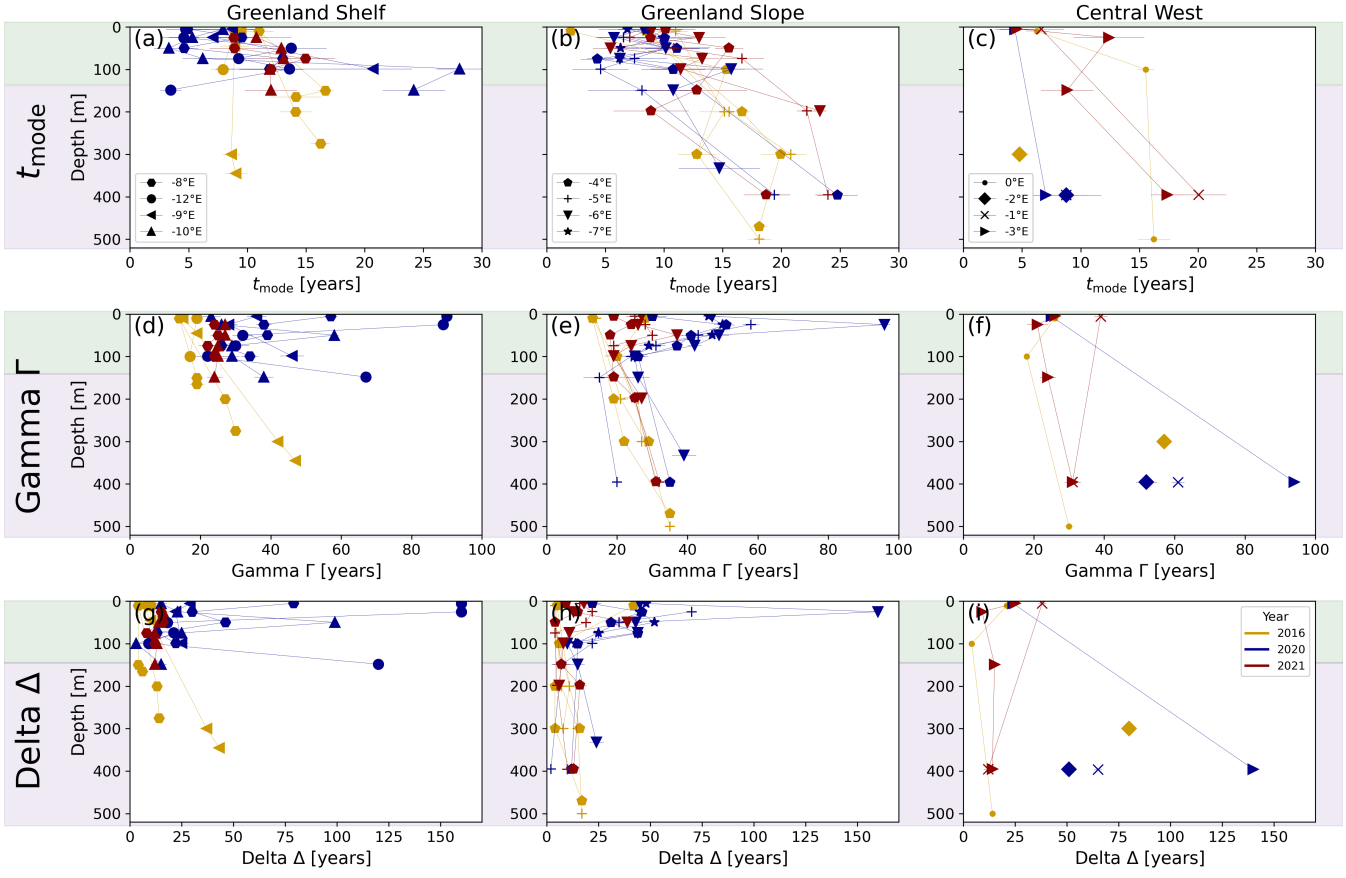

Figure 7. TTD parameters t_{mode} (a-c), Γ (d-f), and Δ (g-i) divided in the three regions of the Greenland Shelf (left), the Greenland Slope (middle), and Central West (right). Results are shown for Polar Water I and Arctic Atlantic Water for the years 2016 (yellow), 2020 (blue), and 2021 (red). The TTD calculations for the surface (green background) followed a different method than at mid-depth (purple background) (see section 2.3.3).

The Greenland Slope showed the most consistent t_{mode} ages throughout the Polar Water I layer (Fig. 7b), similar to the consistent tracer ages in that region. In contrast, the Greenland Shelf exhibited greater variability, particularly in 2020, with t_{mode}

https://doi.org/10.5194/egusphere-2026-2020
Preprint. Discussion started: 21 April 2026

ages increasing with depth (Fig. 7a and Fig. A6a). In the Central West region, t_{mode} ages were lower than those observed at the Greenland Shelf and Slope. Especially in 2020, a subsurface minimum was observed in t_{mode} ages at the Greenland Shelf and Slope at around 50 m depth, which corresponded to a maximum in Γ and Δ in the same depth range. Generally, t_{mode} ages were lowest in 2020 whereas mean ages and the mixing parameter Δ were highest in 2020 throughout the Polar Water I layer (Fig. A6a,b,c).

Several samples deviated from the general pattern. On the Greenland Shelf, a notably low t_{mode} age was recorded at station -12° E (150 m depth) and elevated t_{mode} ages were observed at stations -9° E and -10° E at depths of 100–150 m, which is discussed in section 4.2. For several depths at station -12° E, as well as for one sample from station -6° E (25 m depth), high values for Γ and Δ were apparent.

4 Discussion

4.1 The Role of Mixing in Polar Surface Water Age Estimations

Circulation timescales in the surface Polar Water layer based on anthropogenic radionuclides have historically been estimated using tracer ages derived from the binary mixing model (Wefing et al., 2019, 2021; Smith et al., 2011; Lin et al., 2023a; Casacuberta and Smith, 2023). Tracer ages fundamentally exclude the mixing of water masses carrying different travel times (see section 2.3.2). In contrast, the TTD approach explicitly incorporates the effect of mixing (see section 2.3.4) and provides more comprehensive metrics like the mean age (Γ) and the most probable age (t_{mode}).

This study represents the first application of the TTD model to the surface layer using anthropogenic radionuclides, with the physical consistency of our results validated by the observed depth-dependency in t_{mode} ages. We observed significantly lower ages in the surface layer compared to the mid-depth layer—a discrepancy that is mechanistically consistent with the distinct forcing mechanisms of the region: the surface layer is driven by ocean surface wind stress, whereas the mid-depth layer is largely topographically steered and inherently slower (Lique et al., 2015). These findings align closely with Lagrangian particle tracking studies (Lique et al., 2010), which reported surface transport times of 4–9 years compared to mid-depth returns of up to 25 years. This pattern is further corroborated by Dörr et al. (2026), who found surface timescales predominantly under 10 years and mid-depth timescales often exceeding 20 years. Similar depth-dependent timescales have been substantiated by earlier transient tracer studies (^{3}H, ^{3}He) (Ostlund and Hut, 1984; Ekwurzel et al., 2001; Pasqualini et al., 2024) and independent modeling (Popova et al., 2013; Pemberton et al., 2014; Karcher and Oberhuber, 2002). The robust agreement with historical data reinforces confidence in our application of the TTD model to the surface layer and the model's general ability to capture the fundamental dynamics of the Fram Strait outflow.

https://doi.org/10.5194/egusphere-2026-2020
Preprint. Discussion started: 21 April 2026

To unify the concept of circulation timescales across both the surface and mid-depth layers, we compared the results of the binary mixing model and the TTD model (Fig. 8). Across all three years, a general correspondence was observed, with the alignment of data points along the one-to-one line between tracer age and the TTD parameters (t_{mode}, Γ). Crucially, tracer ages agree well with t_{mode} and Γ when mixing is minimal (i.e., low Δ values). This aligns with the finding of Smith et al. (2011), who observed good agreement between tracer ages and t_{mode} for samples exhibiting advective characteristics at mid-depth. Three samples in 2020 (at $-9°$ E/$-10°$ E) showed particularly good agreement between tracer ages and t_{mode} (highlighted in red in Fig. 8b), suggesting that this older water parcel (discussed in section 4.2) experienced little mixing (Δ between 3 and 24 years, with the lowest Δ showing the best fit). Under these advective conditions, the binary mixing model provides a realistic approximation of circulation timescales.

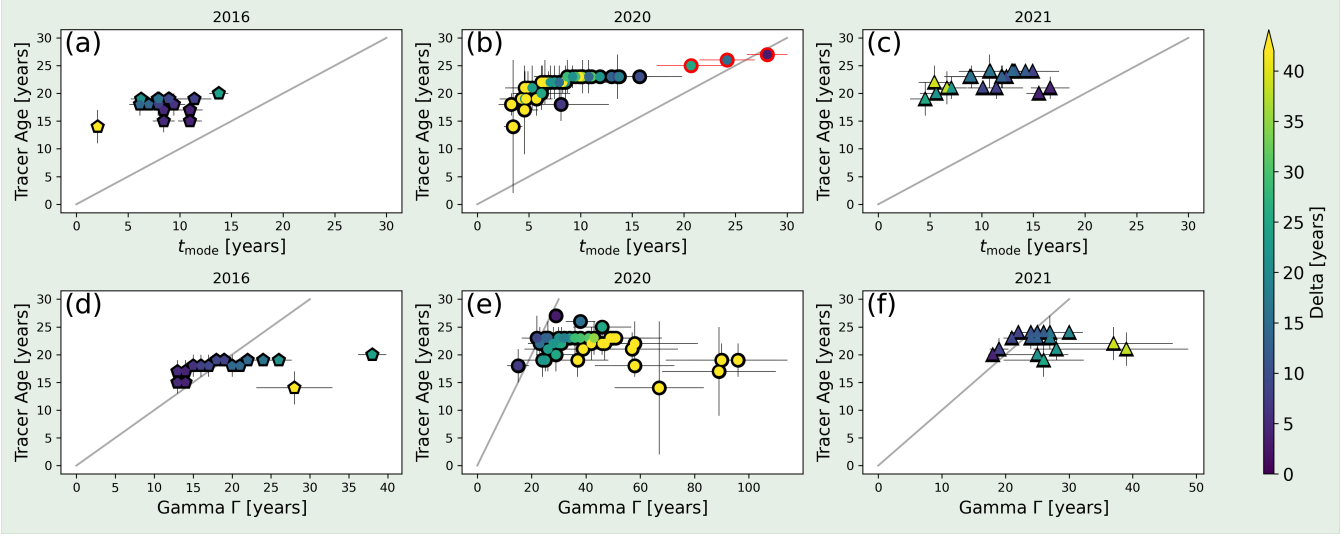

Figure 8. Scatter plot comparing surface Polar Water I (indicated by green background) tracer ages derived from the binary mixing model model with t_{mode} ages (a,b,c) and Γ (d,e,f; note different x-axis limits) obtained from the TTD model for the years 2016, 2020, and 2021. Data points are color-coded according to their corresponding Δ values from the TTD model, representing the degree of mixing. The gray diagonal line indicates the 1:1 relationship between the two age estimates. The samples highlighted with a red ellipse are situated at $-4°$ E and $-5°$ E.

Systematic deviations from the 1:1 line (Fig. 8) correlate with elevated Δ values, confirming that mixing drives model divergence. Specifically, tracer ages underestimate Γ but overestimate t_{mode}. This bias stems from the mixing-induced elongation of the $G(t)$ tail in the probability density function (see examples in Fig. 3b with Δ's of 10 and 20 years): tracer ages are less sensitive to the presence of older water parcels than the mean ages (Γ) (Haine and Hall, 2002), yet are more influenced by it than the t_{mode} age corresponding to the peak of the probability density function (Waugh et al., 2002). Although previous studies, such as Smith et al. (2011), argued that tracer ages are justified at the surface due to its predominantly advective flow and expected narrow $G(t)$ distribution, our results show that mixing (Δ) is not negligible in Polar Water in the Fram Strait, and therefore

https://doi.org/10.5194/egusphere-2026-2020
Preprint. Discussion started: 21 April 2026

tracer ages deviate from t_{mode}. This highlights a fundamental limitation: tracer age profiles appear more uniform than the TTD parameters (compare Fig. 6 to Fig. 7), but this uniformity is misleading. Since water parcels in the Fram Strait are ultimately the result of multiple transit times due to the merging of various branches of different origin, the TTD model, which explicitly accounts for this range of possible transit times, provides a better representation of the complex ocean transport processes. As sea ice retreats, more momentum will be transferred to the ocean, leading to more turbulence and increased mixing (Morison et al., 1985; Martin et al., 2014; Muilwijk et al., 2024; Brown et al., 2025). Therefore, it will become increasingly important to account for mixing when calculating surface layer circulation timescales across the Arctic Ocean and Fram Strait.

Apart from the limitation of the binary mixing model to capture circulation timescales when mixing is large, Waugh et al. (2003) showed that changes in tracer ages do not necessarily imply temporal changes in the circulation. This is because the calculated tracer ages are not fundamental timescales of the flow due to the transient nature of the circulation (Waugh et al., 2003; Haine and Hall, 2002). As also pointed out by Smith et al. (2011), binary mixing models and their related tracer ages are inherently limited in their ability to capture temporal dynamics. This was recently confirmed by Kumamoto et al. (2024), who related an observed increase in tracer ages to model limitations rather than actual longer circulation timescales by comparing the results to TTD estimates. Since the TTD model captures that each water parcel is ultimately the result of a distribution of multiple transit times (Haine and Hall, 2002; Waugh et al., 2003), we suggest that TTD parameters are the superior tool to characterize the flow field and its temporal evolution. Therefore, the subsequent discussions on the origin of water masses (section 4.2) and on the temporal dynamics of circulation (section 4.5) will rely exclusively on the TTD parameters.

4.2 Variability of Water Mass Origin in Polar Water between 2016 and 2021

Unraveling the provenance of Polar Water outflowing through Fram Strait is essential for understanding upstream dynamics and the freshwater export. To this end, we contextualize the ^{129}I and ^{236}U concentrations observed in Polar Water I in 2016, 2020, and 2021 against upstream tracer signatures from distinct Arctic Ocean regions (Fig. 9).

The Polar Water I outflow through Fram Strait reflects a composite signal originating both from the Amerasian and Eurasian Basins. In the Amerasian Basin, Pacific Water entering through the Bering Strait carries predominantly the global fallout tracer signature and mixes with Atlantic-derived waters originating from the Eurasian Basin. These Atlantic-derived waters transport diluted signals from NRPs, and their contribution to the Polar Water in the Amerasian basin remains minor (< 5 %) (Payne et al., 2024), as illustrated in Fig. 9 (black markers with yellow contours). In contrast, waters entering through the WSC, carry a tracer signature shaped by a mixture of Atlantic Water and NCC water. Part of this inflow recirculates within Fram Strait as Recirculating Atlantic Water and subducts beneath Polar Water due to its higher density and joins the EGC at intermediate depths (Hattermann et al., 2016; Appen et al., 2016; Hofmann et al., 2021). Therefore, we do not consider this inflow to be an influencing factor of the observed signal in Polar Water, apart from samples located close to the front between outflowing Polar Water and inflowing WSC waters (approximately east of the prime meridian). In the Eurasian Basin, Polar Waters

https://doi.org/10.5194/egusphere-2026-2020
Preprint. Discussion started: 21 April 2026

do not reflect a pure NCC signature but rather a diluted signal resulting from mixing with Atlantic waters (originating from the North Atlantic Current) that carry global fallout tracer concentrations. These upstream characteristics (black markers with green contours in Fig. 9) exhibit pronounced temporal variability between 2011 and 2021, driven by the transient nature of the tracer input functions (Fig. 2). A similar temporal evolution is observed in the Amerasian Basin (2015–2021), along with a spatial gradient marked by increasing ^{129}I concentrations toward Fram Strait. This pattern reflects the progressive influence of Eurasian Basin waters mixing into the Makarov Basin (Fig. 9).

https://doi.org/10.5194/egusphere-2026-2020
Preprint. Discussion started: 21 April 2026

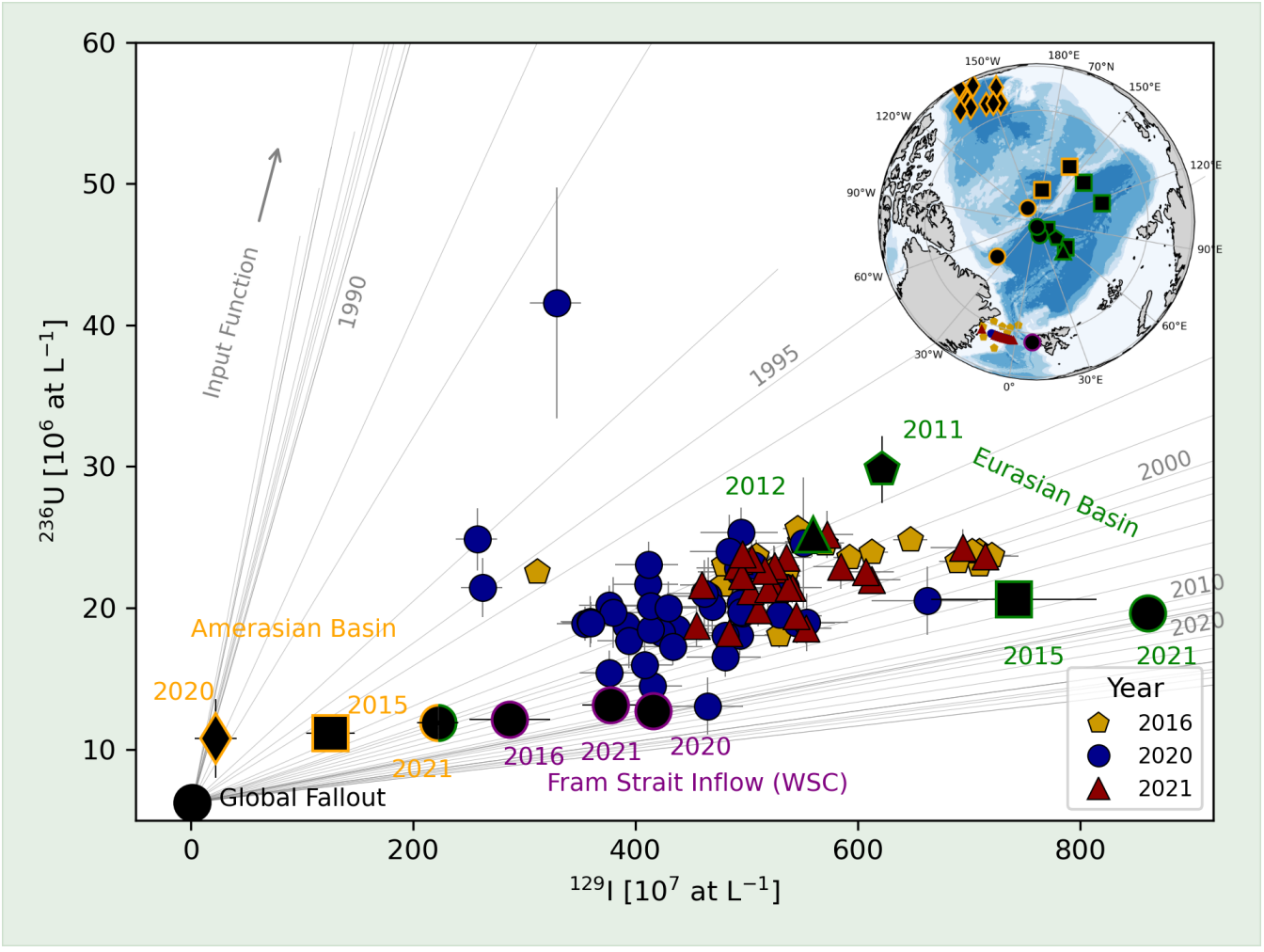

Figure 9. Polar Water I samples from 2016 (yellow), 2020 (blue), and 2021 (red) are displayed in the ^{129}I against ^{236}U tracer space. Previous measurements with the same densities as Polar Water I from 2011, 2012, 2015, 2020, and 2021 are shown as yearly averaged concentrations separately for Amerasian and Eurasian stations. Amerasian-origin waters (orange outline) are represented by samples taken from the Canadian and Makarov Basins, sampled during different expeditions in 2015 (stations 96, 101, and 134 from Casacuberta et al. (2018), squares), 2020 (all stations from Payne et al. (2024), diamonds), and 2021 (stations 28 and 46 from Wefing et al. (2025), circles). Eurasian-origin waters (green outline) are represented by stations in the Amundsen and Nansen Basins, sampled in 2011 (station 212 from Casacuberta et al. (2016), pentagon), 2012 (station 378 from Casacuberta et al. (2016), triangle), 2015 (stations 68, 81, 117, and 125 from Casacuberta et al. (2018), squares), and 2021 (stations 16 and 20 from Wefing et al. (2025), circles). The global fallout tracer signature is indicated as a black circle (1.16×10^7 at L^{-1} for ^{129}I and 6.25×10^6 at L^{-1} for ^{236}U (Snyder et al., 2010; Chamizo et al., 2022)). Inflowing WSC waters (purple outline) are represented as averaged tracer signatures of the upper 100 m at 7° E /8° E in 2016, 2020, and 2021. The surface NCC input function is shown as grey lines with some specific years for orientation. The inlet map shows the geographical location of the samples and upstream tracer signatures.

https://doi.org/10.5194/egusphere-2026-2020
Preprint. Discussion started: 21 April 2026

The Polar Water I samples from 2016, 2020, and 2021 plot largely between the Amerasian and Eurasian tracer signatures, confirming that the outflow is a mixture of these sources (Fig. 9). However, the proportion of the contribution of these two basins varies on an interannual basis. In 2016 and 2021, Polar Water I samples cluster closer to the Eurasian-origin stations, indicating a dominant Eurasian influence. This finding is consistent with Wefing et al. (2022) and is further corroborated by Karpouzoglou et al. (2022), who observed relatively low freshwater transport in 2016—a signal characteristic of Eurasian Basin source waters, as Amerasian-origin waters typically carry a more pronounced freshwater signature derived from Pacific inflow and the Beaufort Gyre. In contrast, 2020 exhibits a marked shift toward the Amerasian-origin endmember. We exclude local dilution by sea-ice melt or meteoric water as the primary driver of this shift, as all samples were salinity-normalized (to $Sal_{ref} = 34.8$, see section 2.3.2). Instead, this anomaly aligns with the trend reported by Wefing et al. (2022), who attributed a shift in tracer signals between 2016 and 2018/2019 to an increasing Amerasian contribution. Our data suggests this trend continued into 2020, likely linked to the release of freshwater accumulated in the Beaufort Gyre—a primary reservoir of Amerasian water that showed an increasing freshwater content in the 2000s and 2010s (Giles et al., 2012; Proshutinsky et al., 2019; Lin et al., 2023b)—towards Fram Strait around 2019 (Wang et al., 2024). Finally, Planat et al. (2025) found negligible Pacific Water export through Fram Strait between 2005 and 2017, a finding compatible with our observation of a pulse of Amerasian water arriving only in 2020, subsequent to the post-2019 release event described by Wang et al. (2024).

Distinguishing between Atlantic- and Pacific-origin waters in the surface Arctic Ocean is complex and requires multiple complementary approaches. While nutrient-based tracers have historically been used to track Pacific Water variability in Fram Strait (Dodd et al., 2012; Falck et al., 2005; Jones et al., 2008), their conservative behavior has been questioned in several studies (Alkire et al., 2015, 2019; Bauch et al., 2011). In this context, ^{129}I provides an additional, independent constraint, owing to the approximately eight-fold concentration contrast between Amerasian surface waters, which reflect the low-level global fallout signature from the Pacific, and Eurasian surface waters, which carry a strong Atlantic ^{129}I signal. Future assessments of water mass origin in Fram Strait would benefit from a comprehensive multi-tracer approach. Combining ^{129}I and ^{236}U with other parameters such as CDOM, delta-Oxygen-18 (δ^{18}O), Neon (Ne), and Neodymium (Nd) could significantly improve source disentanglement (Dodd et al., 2012; Lin et al., 2023a; Heuzé et al., 2023; Pérez-Tribouillier et al., 2025). For instance, Nd has already been used to distinguish Pacific from Atlantic waters in both the Fram Strait (Laukert et al., 2017) and the central Arctic Ocean (Paffrath et al., 2021). Gallium has also been investigated as a water mass tracer in the central Arctic (McAlister and Orians, 2015; Whitmore et al., 2020). Ultimately, integrating ^{129}I and ^{236}U with these tracers (especially CDOM, δ^{18}O, Ne, and Nd) would provide a more robust framework for delineating freshwater sources than the salinity normalization method employed here (Dodd et al., 2012; Granskog et al., 2012; Pérez-Tribouillier et al., 2025).

4.3 Divergence from Advective Flow in 2020: Enhanced Mixing and Age Broadening Across the Water Column

The shift in water mass provenance towards a higher contribution of Amerasian Basin waters in Polar Water I in 2020 is coupled with an increase in mixing, as revealed by the TTD parameters (Fig. 10a-d). Similar temporal trends are observed for

https://doi.org/10.5194/egusphere-2026-2020
Preprint. Discussion started: 21 April 2026

samples from the mid-depth Arctic Atlantic Water (Fig. 10e-h), despite the limited sampling resolution. The year 2020 is characterized by a substantial increase in the mixing parameter Δ (Fig. 10a and e), as well as the mean age Γ (Fig. 10b and f). This indicates that the Amerasian-influenced water parcels in Polar Water I as well as the Arctic Atlantic Water experienced a more complex transit history with a broader range of ages compared to the more coherent, advective flow of 2016 and 2021. This interpretation is reinforced by elevated Δ/Γ ratios in 2020 (Polar Water I range: 0.1–1.8, Arctic Atlantic Water range: 0.1–1.5; see Fig. 10c and g), pointing to less advective transport during this period. Finally, the observed reversal to Eurasian-dominated source waters in 2021 supports the hypothesis by Smith et al. (2021) that the Arctic Oscillation peak in 2020 triggered a return to a cyclonic regime. Such a regime is associated with a weaker Beaufort Gyre and fundamental structural changes in the surface Arctic circulation, favoring the Atlantic-derived Eurasian signals observed again in Polar Water I in 2021. Based on our findings, we suggest that these changes were not limited to the surface layer but extended to the mid-depth Atlantic layer.

https://doi.org/10.5194/egusphere-2026-2020
Preprint. Discussion started: 21 April 2026

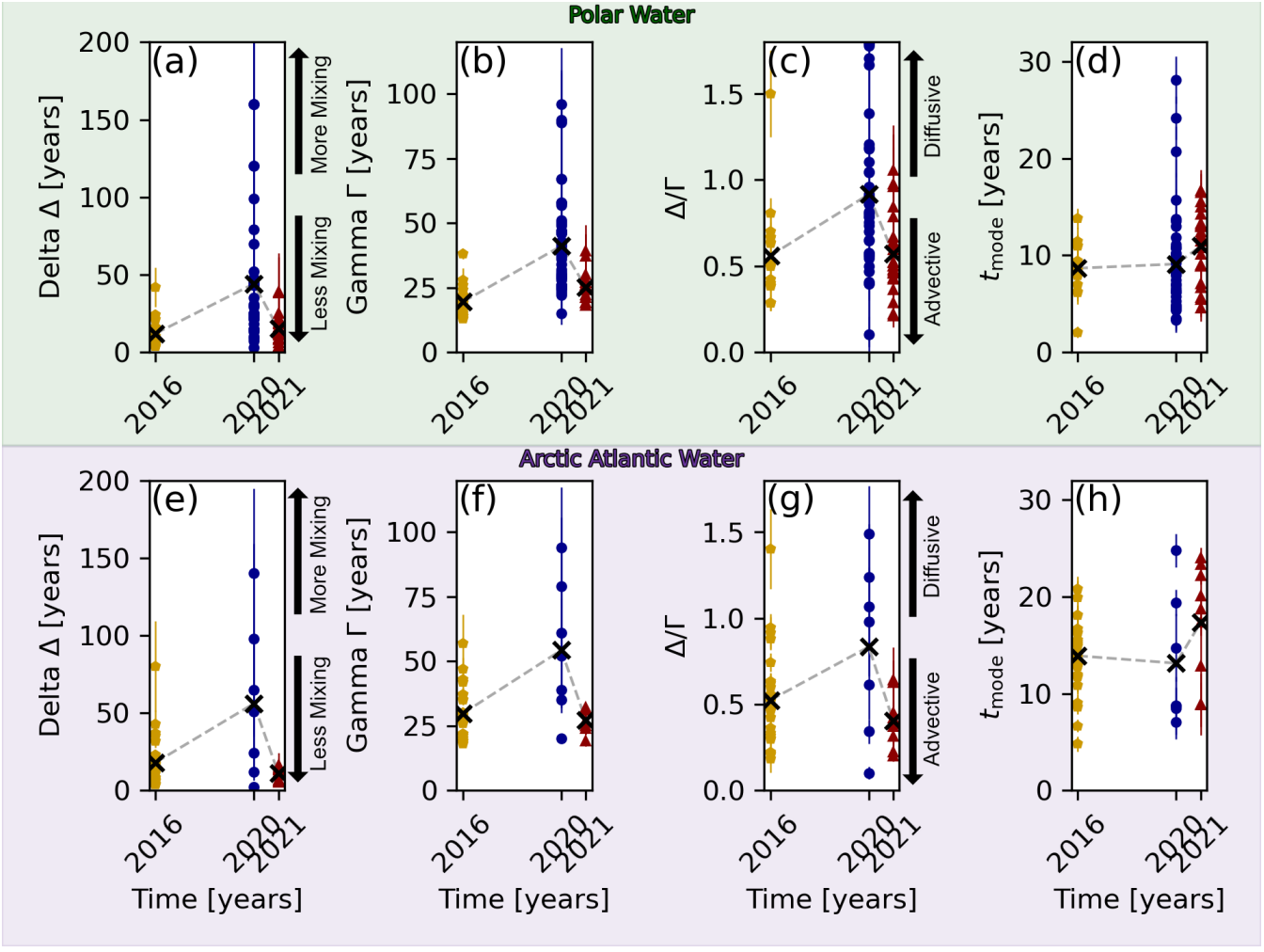

Figure 10. The results of the TTD model are shown for the Polar Water I surface layer (a-d, green background) and Arctic Atlantic Water mid-depth layer (e-h, purple background) for three years, 2016 (yellow), 2020 (blue), and 2021 (red). Four TTD parameters are shown: t_{mode} (a,e), Γ (b,f), Δ (c,g), and Δ/Γ (d,h). The black crosses indicate the respective average values.

4.4 Convergence of Distinct Water Masses in 2020: Identifying Canada Basin and Shelf Signatures

The 2020 dataset features both highest and lowest ^{236}U concentrations measured across all years discussed in this study and a larger range of ^{129}I concentrations compared to 2016 and 2021. This is also reflected in the large range of the TTD parameters obtained for 2020, both for Polar Water I and Arctic Atlantic Water (Fig. 10). A more detailed analysis of the highly heterogeneous 2020 dataset reveals substructures within the outflow, highlighting the complexity of the region.

https://doi.org/10.5194/egusphere-2026-2020
Preprint. Discussion started: 21 April 2026

Three samples in 2020 (at $-9°$ E to $-10°$ E, 100–150 m depth, see Fig. 9) exhibited anomalously high ^{236}U concentrations relative to ^{129}I. Comparison with the time-dependent input function (Fig. 2) reveals that such elevated ^{236}U levels are influenced to old source waters. This signature identifies a distinct water parcel with a significantly greater age (tracer age: 25–27 years; t_{mode}: 21–28 years) than the surrounding water. We attribute this to a parcel that followed a longer circulation route through the Canada Basin, consistent with the "long path" hypothesis often associated with low-temperature anomalies in this region (Rudels et al., 2000). Although two samples indeed showed lower conservative temperatures ($-1.51°$ C and $-1.64°$ C) than the Polar Water average ($-1.49°$ C), the third sample was higher ($-0.92°$ C); consequently, conservative temperature may not be a definitive indicator for the long-path hypothesis in this context.

Conversely, samples with the lowest ^{236}U concentrations in 2020 ($13 \pm 2 \times 10^6$ at L^{-1}) and relatively low ^{129}I concentrations (around 400×10^7 at L^{-1}) likely reflect waters that recirculated on the Greenland Shelf, potentially within the East Greenland Coastal Current, where they underwent dilution. This interpretation is supported by their geographical location on the shelf (primarily at $-12°$ E, see Fig. 9). While eddy transport of Recirculating Atlantic Water onto the shelf—a mechanism described by Hattermann et al. (2016)—offers an alternative explanation, Recirculating Atlantic Water typically subducts beneath the cold, fresh Polar Water. The absence of both elevated temperatures (characteristic of Recirculating Atlantic Water) and low salinities (indicative of fresh meltwater) further supports the shelf recirculation hypothesis. As station $-12°$ E was not sampled during the 2021 expedition (see Fig. 4), the apparent absence of this low-concentration signal in 2021 likely results from spatial sampling bias rather than the temporal disappearance of this shelf feature.

Low t_{mode} ages obtained for Arctic Atlantic Water samples in central Fram Strait in 2020 were coupled with high Δ values (Fig. 7c,i and Fig. 8b) and point to mixing with Recirculating Atlantic Water, carrying very young tracer signals. These findings are also supported by the distribution in TS-space.

The substantial range in t_{mode} ages observed within the surface Polar Water I and mid-depth Arctic Atlantic Water masses (Fig. 10d,h) underscores the convergence of different water masses from the central Arctic and the Nordic Seas, the latter recirculating in Fram Strait as Recirculating Atlantic Water. Rather than a unimodal approach, this complex regime is likely better represented by bimodal or multimodal TTDs capable of capturing multiple peaks from mixing water masses. Such approaches have been increasingly advocated for other regions (Haine and Hall, 2002; Peacock and Maltrud, 2006; Chouksey et al., 2022; Guo et al., 2025) and were recently applied to ^{129}I and ^{236}U to distinguish branches from the central Arctic and Canada Basin (Wefing et al., 2025). Within the Fram Strait, the additional influence of the WSC suggests that a trimodal TTD structure may be necessary to fully resolve the regional circulation. However, this is beyond the scope of this study and should be further elaborated in future work with more data available to resolve the contributions.

https://doi.org/10.5194/egusphere-2026-2020
Preprint. Discussion started: 21 April 2026

4.5 Drivers of the 2021 Mode Age Elevation: Assessing Evidence for Circulation Slowdown and Path Extension

To address the temporal variability of circulation timescales between 2016 and 2021, we use the most probable age (t_{mode}), which serves as a robust metric for assessing the temporal evolution of advective circulation timescales, as also pointed out by Wefing et al. (2021).

The data suggest a shift toward longer circulation timescales and/or pathways in 2021 (Fig. 10a,e) for the surface and the mid-depth Atlantic layer. While the mean t_{mode} remained relatively constant from 2016 to 2020, it exhibited an increase in 2021 across both layers, a trend more pronounced at mid-depth. This shift is further evidenced by the distribution of extreme values in the mid-depth layer. In 2016, the majority of t_{mode} values ranged between 10 and 20 years. In contrast, despite lower sampling density in 2021, we observed multiple samples with t_{mode} values exceeding 20 years. This shift in the age distribution suggests either a deceleration of the circulation and/or a lengthening of the transport pathways reaching the Fram Strait.

The observation of increasing circulation timescales and/or longer pathways in the surface layer presents a complex picture when viewed against established literature. Our results for Polar Water I confirm the elevated circulation timescales observed in Fram Strait in 2021 by Lin et al. (2023a). However, a slowdown of the surface circulation does not align with the general consensus that ongoing sea-ice decline increases ocean surface stress, thereby strengthening Arctic geostrophic currents (Meredith et al., 2019). Such intensification has been consistently supported by satellite data, model predictions, and mooring observations (Muilwijk et al., 2024; Polyakov et al., 2020b; Wang et al., 2022). A different explanation for the increased transit times we observed in 2021 is a change towards longer, more circuitous pathways. This interpretation aligns with the narrative of highly variable Arctic Ocean surface trajectories described in previous studies (Wilson et al., 2021), suggesting that a shift in pathway length, rather than a reduction in current velocity, drives the observed signal.

In contrast, the findings of elevated mode ages in the mid-depth layer in 2021 are well-supported by independent evidence of a recent circulation slowdown. Our results align with reports of increased circulation timescales in the central Arctic Ocean between 2011 and 2021 (Wefing et al., 2025), decreasing ADCP velocities in the EGC (Karpouzoglou et al., 2022), increased mean ages attributed to a weakening boundary current from 2005 to 2021 (Gerke et al., 2024), and increased circulation timescales in the Fram Strait in 2021 (Lin et al., 2023a). Mechanistically, the specific increase observed in 2021 may be linked to a known transient period of reduced flow in the Siberian Arctic Ocean between late 2015 and early 2018 (Polyakov et al., 2025a). While the 2016 circulation timescales were likely unaffected by this event due to insufficient tracer propagation time, the lagged signal would likely reach the Fram Strait region by 2020 and 2021, contributing to the observed increase in ages. If this temporary pulse is the primary driver, future observations should reveal a reversal toward shorter circulation timescales, consistent with recent evidence of a strengthening Arctic overturning circulation (Årthun et al., 2026).

https://doi.org/10.5194/egusphere-2026-2020
Preprint. Discussion started: 21 April 2026

5 Conclusions and Outlook

This study utilized the combination of anthropogenic radionuclide transient tracers ^{129}I and ^{236}U to investigate the origin, degree of mixing, and circulation timescales of water masses exiting the Arctic Ocean through Fram Strait between years 2016 and 2021. Two models were applied to obtain estimates of circulation timescales: the binary mixing model resulting in tracer ages (only applied to surface Polar Water I samples) and the TTD model resulting in mean (Γ) and mode (t_{mode}) ages as well as a mixing parameter (Δ). This model has previously only been applied to radionuclide data from Arctic Atlantic Water and was here for the first time also applied to samples from Polar Water I, after correcting for the dilution with the global fallout signal mainly coming from Pacific origin.

The relationships between tracer ages derived from the binary mixing model and the mean and mode ages from the TTD model were validated for Polar Water I samples exhibiting a strong advective component (low Δ values). However, several Polar Water I samples were dominated by mixing processes (high Δ values) and the ages from the two models did not agree. Our findings therefore suggest that the transport in the surface is not as advective as previously proposed (Smith et al., 2011) and we emphasize that the TTD model, which accounts for a distribution of transit times due to mixing within the flow, is also preferred at the surface to accurately characterize the flow field.

The tracer data revealed significant interannual variability in water mass properties. Specifically, the year 2020 was characterized by a higher proportion of Amerasian Basin waters in the surface Polar Water layer and by a notably higher degree of mixing throughout the water column compared to 2016 and 2021. Our observations also suggest that the central Fram Strait experienced a substantial influence from Recirculating Atlantic Water from the WSC in 2020. Additionally, a small cluster of water samples on the Greenland Shelf region exhibited very old ages consistent with an origin in the Canada Basin. The distinct tracer signature—a low ^{129}I concentration coupled with a high ^{236}U concentration—proved highly effective in identifying these small—scale substructures within the water masses, underscoring the usefulness of ^{129}I-^{236}U as a tracer pair to delineate water mass origins.

Finally, the TTD model suggested increased circulation timescales (t_{mode} ages) for both the surface and mid-depth layers in 2021. While the dataset does not permit assessment of a long-term trend, this observation could be linked to the previously reported period of reduced boundary current flow in the Siberian Shelf region (Polyakov et al., 2025a). If this transient pulse is the cause, circulation timescales may decrease again in the near future.

To address these complex temporal shifts, further tracer-based monitoring at key locations like the Fram Strait is crucial for estimating mean flow developments and complementing the high temporal resolution of current meter observations at specific locations, as highlighted by Pasqualini et al. (2024). A comprehensive multi-tracer study—incorporating ^{129}I, ^{236}U, CFCs, SF_6, and Tritium—would significantly reduce the uncertainties in circulation timescales. Since different tracer combinations

https://doi.org/10.5194/egusphere-2026-2020
Preprint. Discussion started: 21 April 2026

respond uniquely to boundary conditions and source histories (Haine and Hall, 2002; Waugh et al., 2003), integrating them would provide a more robust estimate of transit times, independent of the source history of any single tracer. To refine the application of the TTD model to surface samples, tracer data from upstream regions of Fram Strait would be valuable to better constrain the fraction of Pacific-origin water entering the study region. Overall, strategic and synergistic tracer sampling at the Fram Strait will significantly enhance our ability to monitor, understand, and improve predictive capabilities for the Arctic Ocean circulation regime under a warming climate.

6 Open Research

Data availability.

The CTD data for 2016 was taken from Kanzow and Rohardt (2017).

The CTD data for 2020 and 2021 was taken from Dodd et al. (2022a, b).

The ^{129}I and ^{236}U data for 2016 was taken from Wefing et al. (2019).

The ^{236}U data for 2020 and 2021 was taken from Lin et al. (2023a).

A subset of the ^{129}I data from 2021 has been published in Pérez-Tribouillier et al. (2025)

The ^{129}I data for 2020 and 2021 is available on Zenodo (Scheiwiller, 2026).

https://doi.org/10.5194/egusphere-2026-2020
Preprint. Discussion started: 21 April 2026

Appendix A: Supporting Figures

A1 Intercomparison of ^{236}U between ETH Zurich and DTU

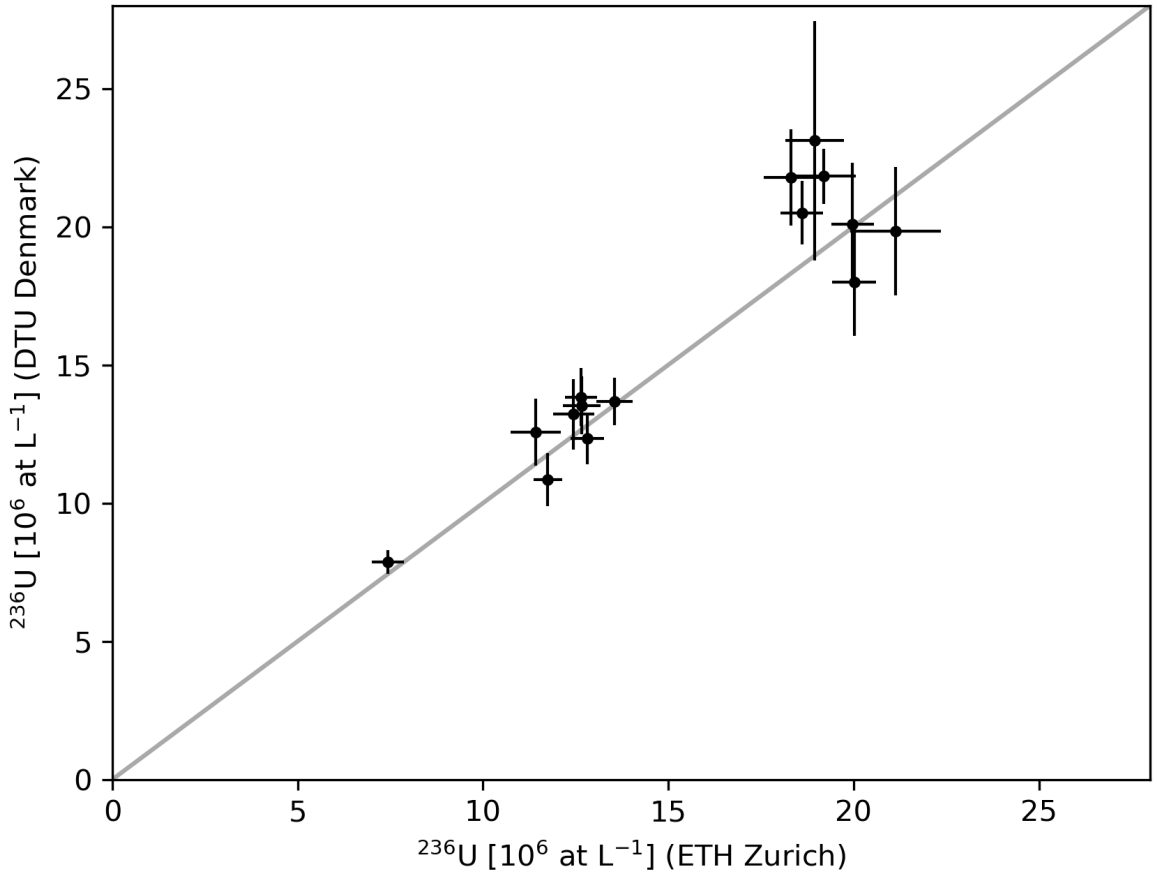

Figure A1. Comparison of ^{236}U concentrations of duplicate samples measured at ETH Zurich and the Technical University of Denmark.

https://doi.org/10.5194/egusphere-2026-2020
Preprint. Discussion started: 21 April 2026

A2 Overview map of Stations in 2016, 2020, and 2021

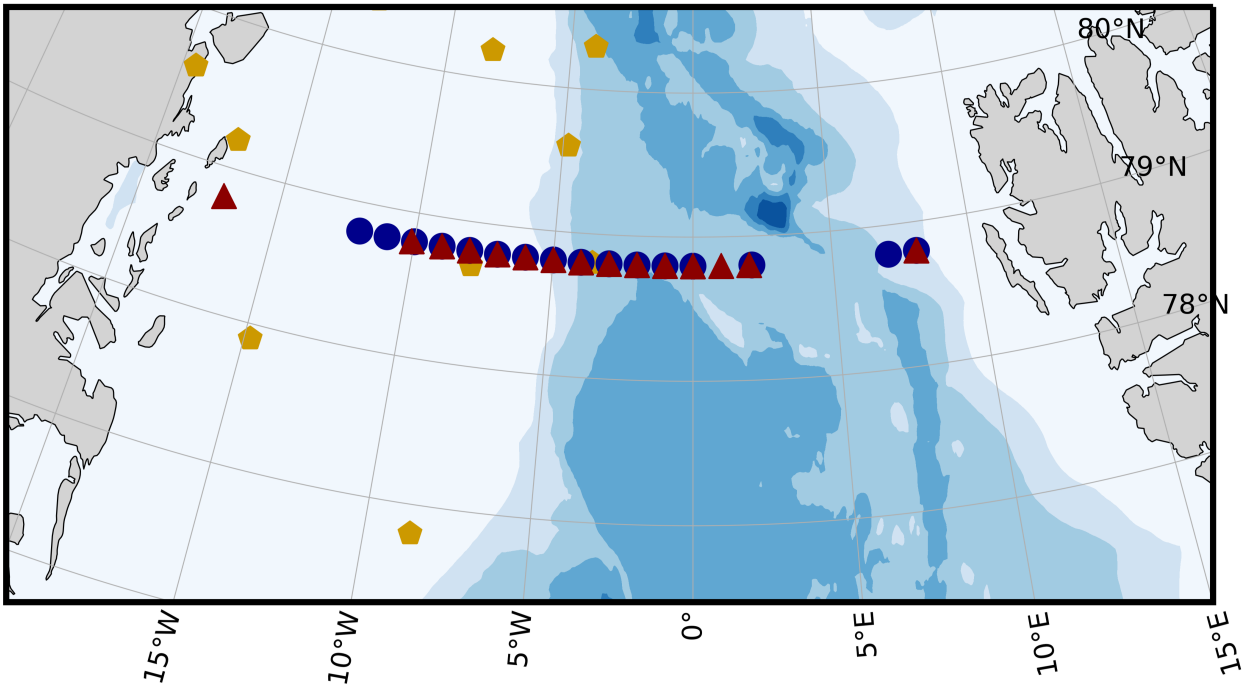

Figure A2. Overview map of all stations in 2016, 2020, and 2021. The data from 2016 is taken from Wefing et al. (2019).

https://doi.org/10.5194/egusphere-2026-2020
Preprint. Discussion started: 21 April 2026

A3 The binary mixing model with data from 2016, 2020, and 2021

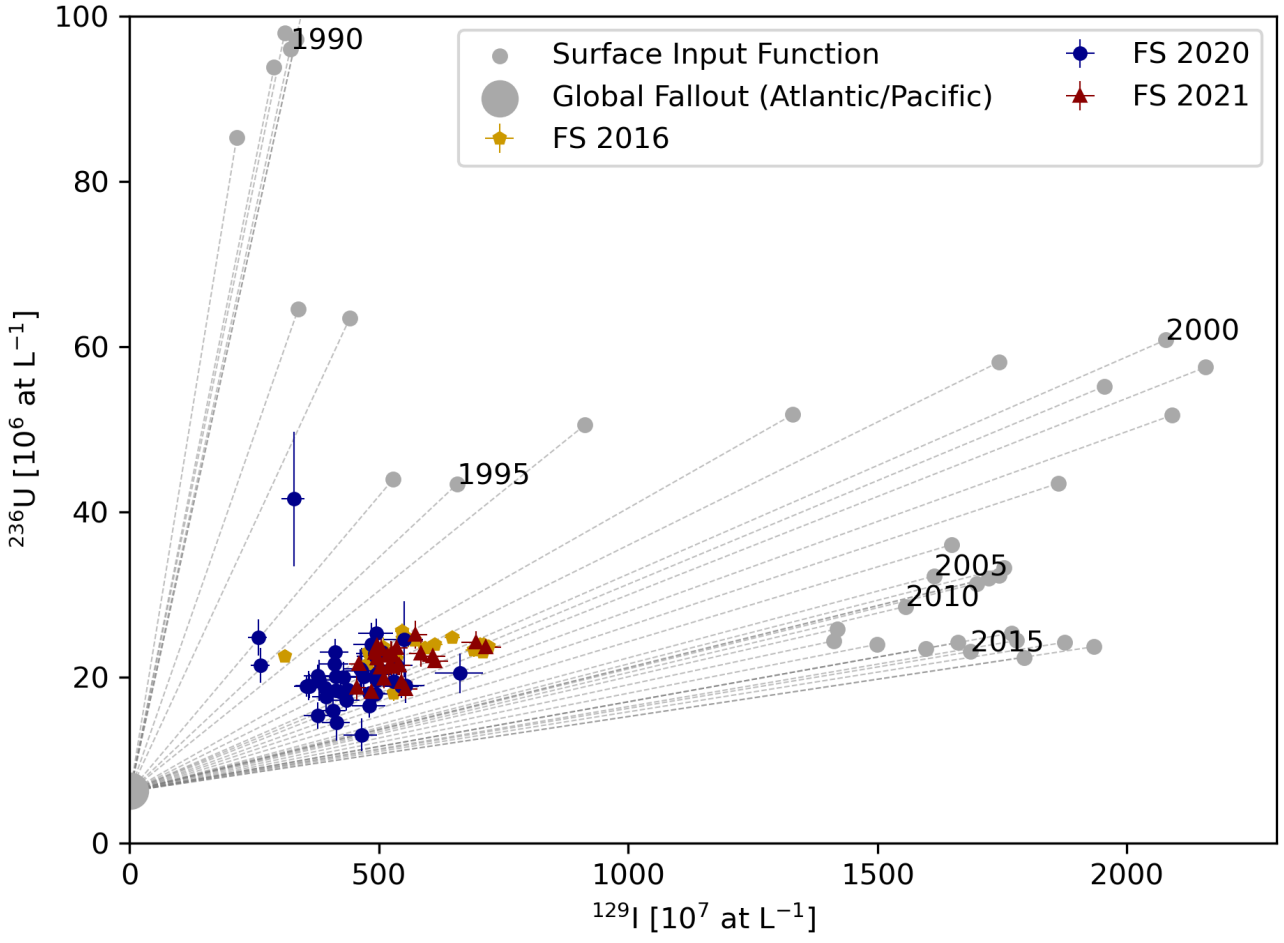

Figure A3. The binary mixing model grid with a constant global fallout background level (large gray point) and a time varying input of ^{129}I and ^{236}U to the surface Arctic Ocean (small gray points). The data for Polar Water I from 2016, 2020, and 2021 is shown on top.

https://doi.org/10.5194/egusphere-2026-2020
Preprint. Discussion started: 21 April 2026

A4 Transit Time Distribution grids with data from 2016, 2020 and 2021

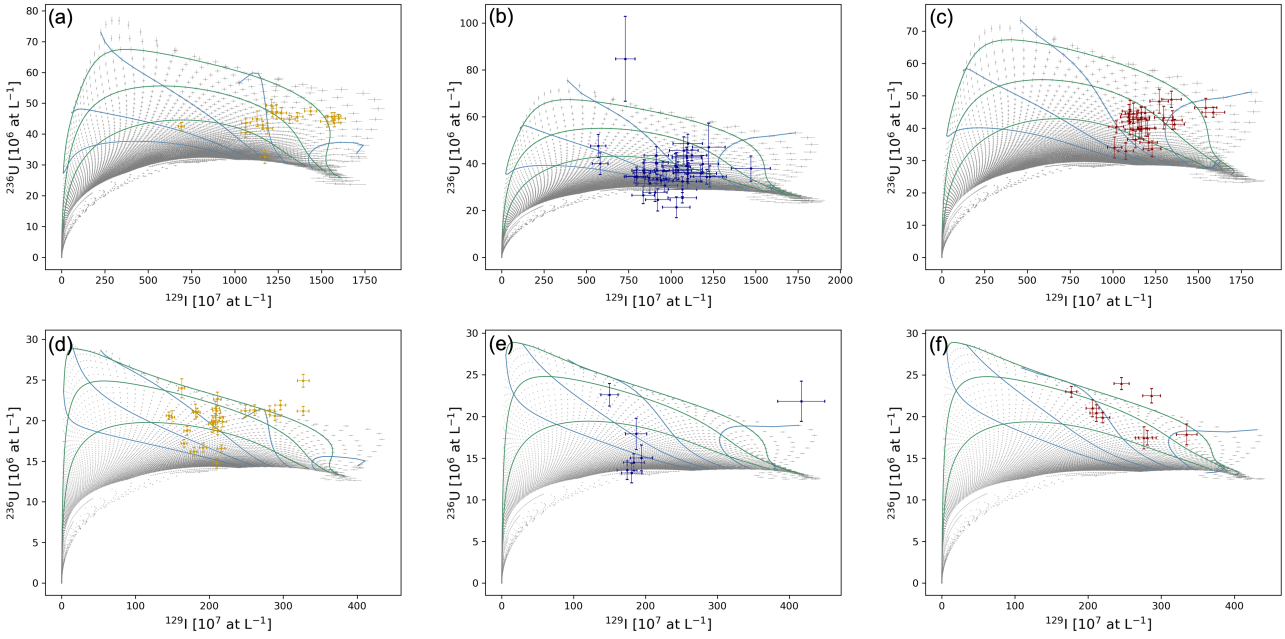

Figure A4. The TTD model grids for 2016 (a,d), 2020 (b,e), and 2021 (c,f) with Polar Water I data shown for the surface (a,b,c) and Arctic Atlantic Water for the mid-depth (d,e,f). The surface data was corrected according to the described method in section 2.3.4 with a 55 % global fallout fraction.

https://doi.org/10.5194/egusphere-2026-2020
Preprint. Discussion started: 21 April 2026

A5 Comparison of Correction Percentages for Surface Transit Time Distributions

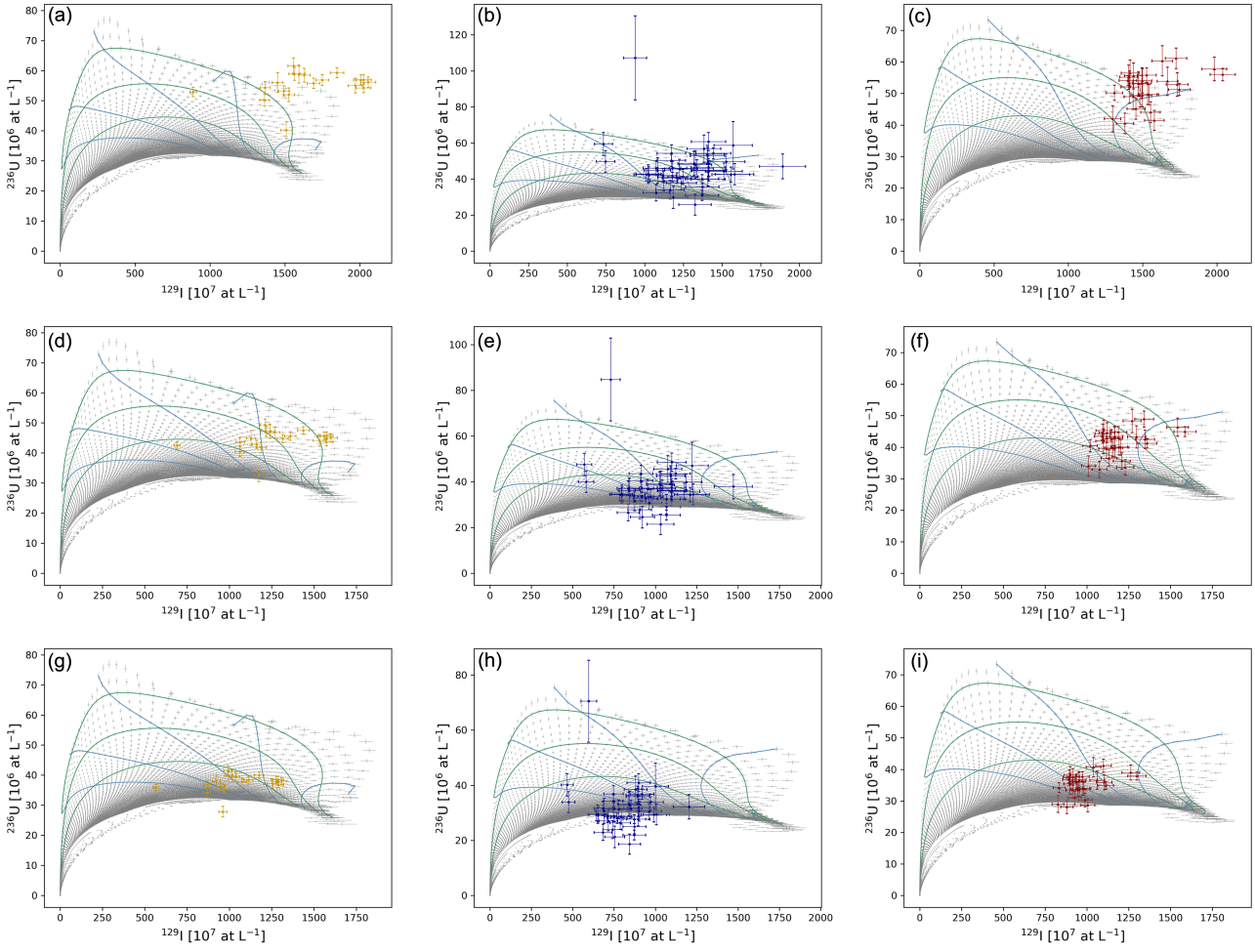

Figure A5. The TTD model grids for 2016 (a,d,g), 2020 (b,e,h), and 2021 (c,f,i) with Polar Water I data shown for the surface. The surface data was corrected according to the described method in section 2.3.4 with a 65 % (a,b,c), 55 % (d,e,f), and 45 % (g,h,i) global fallout fraction to find the best fit.

https://doi.org/10.5194/egusphere-2026-2020
Preprint. Discussion started: 21 April 2026

A6 Transit Time Distribution sections for 2020 and 2021

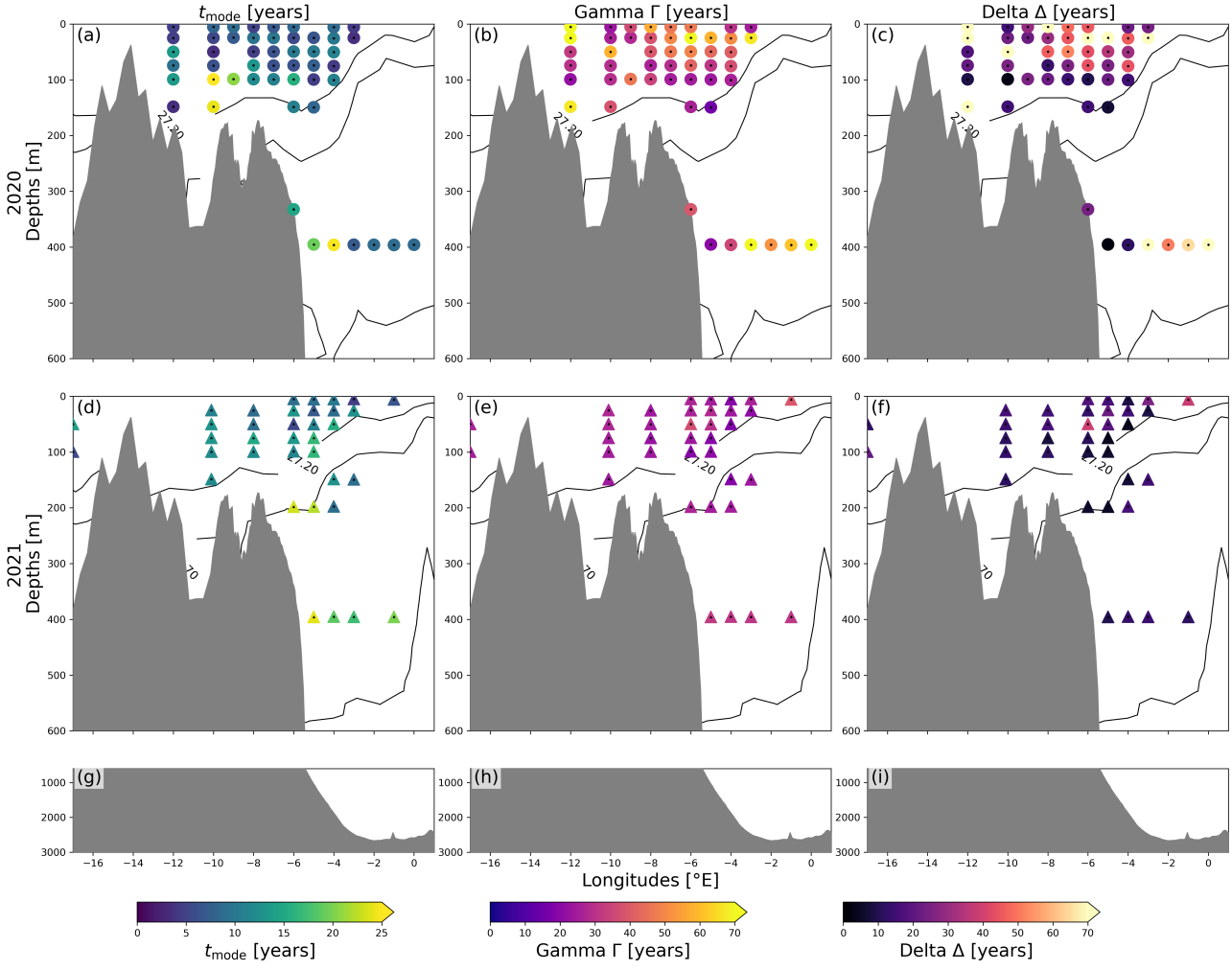

Figure A6. TTD parameters t_{mode} (a,d), Γ (b,e), and Δ (c,f) for 2020 (a,b,c) and 2021 (d,e,f). Results are shown for Polar Water I and Arctic Atlantic Water. Selected σ_0 isopycnals (black) are overlaid.

https://doi.org/10.5194/egusphere-2026-2020
Preprint. Discussion started: 21 April 2026

Author contributions.

MS performed the conceptualization, investigation, data curation, formal analysis, visualization, and wrote the original draft. AMW supported the conceptualization, investigation and data curation and performed writing (review and editing). HPT supported the measurement of data, methodology and performed writing (review and editing). CV supported the measurement of data and methodology. PAD and JPG provided resources and performed writing (review and editing). NC acquired funding, provided resources, supported the conceptualization, investigation, measurements of data, and data curation and performed writing (review and editing).

Competing interests. The authors declare that they have no conflict of interest.

Acknowledgements. The first author received funding from ETH Zürich (Grant 22-2 ETH-028). The work is embedded in the TITANICA project (PI Núria Casacuberta) funded by the European Research Council (ERC) as part of the European Union's Horizon 2020 research and innovation programme (ERC-2020-COG 101001451) and the TRACEATLANTIC project funded by the Swiss National Science Foundation (PR00P2-193091-TRACEATLANTIC). AMW acknowledges funding from the SNSF Postdoc.Mobility fellowship TRACPAC (Project number P500PN_217968). PAD and JPG were supported through funding from the Fram Centre TRIMODAL project. The authors acknowledge the Norwegian Polar Institute and all participants, captain and crew memebers of the Fram Strait Expeditions in 2020 and 2021 onboard the RV Kronprins Haakon for the collaboration and team effort on the vessel. A special thank you goes to Kayley Kündig for the support in the laboratory and all the staff of the Laboratory of Ion Beam Physics who contributed to this project.

https://doi.org/10.5194/egusphere-2026-2020
Preprint. Discussion started: 21 April 2026

References

Aagaard, K.: A synthesis of the Arctic Ocean circulation, Rcun. Cons. int. Explor. Mer, 188, 11–22, 1989.

Aagaard, K. and Reed, R.: Fram Strait: Exchange and dynamics, Eos, Transactions American Geophysical Union, 68, 124–125, 1987.

Aksenov, Y., Ivanov, V. V., Nurser, A. J., Bacon, S., Polyakov, I. V., Coward, A. C., Naveira-Garabato, A. C., and Beszczynska-Moeller, A.: The Arctic Circumpolar Boundary Current, Journal of Geophysical Research: Oceans, 116, 9017, 2011.

Alfimov, V., Aldahan, A., Possnert, G., and Winsor, P.: Anthropogenic iodine-129 in seawater along a transect from the Norwegian coastal current to the North Pole, Marine Pollution Bulletin, 49, 1097–1104, 2004.

Alfimov, V., Aldahan, A., and Possnert, G.: Water masses and 129I distribution in the Nordic Seas, Nuclear Instruments and Methods in Physics Research Section B: Beam Interactions with Materials and Atoms, 294, 542–546, 2013.

Alkire, M. B., Morison, J., and Andersen, R.: Variability in the meteoric water, sea-ice melt, and Pacific water contributions to the central Arctic Ocean, 2000-2014, Journal of Geophysical Research: Oceans, 120, 1573–1598, 2015.

Alkire, M. B., Rember, R., and Polyakov, I.: Discrepancy in the Identification of the Atlantic/Pacific Front in the Central Arctic Ocean: NO Versus Nutrient Relationships, Geophysical Research Letters, 46, 3843–3852, 2019.

Appen, W. J. V., Schauer, U., Hattermann, T., and Beszczynska-Möller, A.: Seasonal Cycle of Mesoscale Instability of the West Spitsbergen Current, Journal of Physical Oceanography, 46, 1231–1254, 2016.

Bates, N. R., Moran, S. B., Hansell, D. A., and Mathis, J. T.: An increasing CO2 sink in the Arctic Ocean due to sea-ice loss, Geophysical Research Letters, 33, 23 609, 2006.

Bauch, D., van der Loeff, M. R., Andersen, N., Torres-Valdes, S., Bakker, K., and Abrahamsen, E. P.: Origin of freshwater and polynya water in the Arctic Ocean halocline in summer 2007, Progress in Oceanography, 91, 482–495, 2011.

Besczynska-Möller, A., Woodgate, R. A., Lee, C., Melling, H., and Karcher, M.: A Synthesis of Exchanges Through the Main Oceanic Gateways to the Arctic Ocean, Oceanography, 24, 82–99, 2011.

Box, J. E., Colgan, W. T., Christensen, T. R., Schmidt, N. M., Lund, M., Parmentier, F. J. W., Brown, R., Bhatt, U. S., Euskirchen, E. S., Romanovsky, V. E., Walsh, J. E., Overland, J. E., Wang, M., Corell, R. W., Meier, W. N., Wouters, B., Mernild, S., Mård, J., Pawlak, J., and Olsen, M. S.: Key indicators of Arctic climate change: 1971–2017, Environmental Research Letters, 14, 045 010, 2019.

Bras, I. L., Straneo, F., Muilwijk, M., Smedsrud, L. H., Li, F., Lozier, M. S., and Holliday, N. P.: How Much Arctic Fresh Water Participates in the Subpolar Overturning Circulation?, Journal of Physical Oceanography, 51, 955–973, 2021.

Brown, N. J., Garabato, A. C. N., Bacon, S., Aksenov, Y., Tsubouchi, T., Green, M., Lincoln, B., Rippeth, T., and Feltham, D. L.: The Arctic Ocean Double Estuary: Quantification and Forcing Mechanisms, AGU Advances, 6, e2024AV001 529, 2025.

Carmack, E. C., Yamamoto-Kawai, M., Haine, T. W., Bacon, S., Bluhm, B. A., Lique, C., Melling, H., Polyakov, I. V., Straneo, F., Timmermans, M. L., and Williams, W. J.: Freshwater and its role in the Arctic Marine System: Sources, disposition, storage, export, and physical and biogeochemical consequences in the Arctic and global oceans, Journal of Geophysical Research: Biogeosciences, 121, 675–717, 2016.

Casacuberta, N. and Smith, J. N.: Nuclear Reprocessing Tracers Illuminate Flow Features and Connectivity Between the Arctic and Subpolar North Atlantic Oceans, 08, 54, 2023.

Casacuberta, N., Christl, M., Lachner, J., van der Loeff, M. R., Masqué, P., and Synal, H. A.: A first transect of 236U in the North Atlantic Ocean, Geochimica et Cosmochimica Acta, 133, 34–46, 2014.

https://doi.org/10.5194/egusphere-2026-2020
Preprint. Discussion started: 21 April 2026

Casacuberta, N., Masqué, P., Henderson, G., van-der Loeff, M. R., Bauch, D., Vockenhuber, C., Daraoui, A., Walther, C., Synal, H. A., and Christl, M.: First 236U data from the Arctic Ocean and use of 236U/238U and 129I/236U as a new dual tracer, Earth and Planetary Science Letters, 440, 127–134, 2016.

Casacuberta, N., Christl, M., Vockenhuber, C., Wefing, A. M., Wacker, L., Masqué, P., Synal, H. A., and van der Loeff, M. R.: Tracing the Three Atlantic Branches Entering the Arctic Ocean With 129I and 236U, Journal of Geophysical Research: Oceans, 123, 6909–6921, 2018.

Chamizo, E., Christl, M., López-Lora, M., Casacuberta, N., Wefing, A. M., and Kenna, T. C.: The Potential of 233U/236U as a Water Mass Tracer in the Arctic Ocean, Journal of Geophysical Research: Oceans, 127, e2021JC017 790, 2022.

Chouksey, M., Griesel, A., Eden, C., and Steinfeldt, R.: Transit Time Distributions and Ventilation Pathways Using CFCs and Lagrangian Backtracking in the South Atlantic of an Eddying Ocean Model, Journal of Physical Oceanography, 52, 1531–1548, 2022.

Christl, M., Lachner, J., Vockenhuber, C., Lechtenfeld, O., Stimac, I., van der Loeff, M. R., and Synal, H. A.: A depth profile of uranium-236 in the Atlantic Ocean, Geochimica et Cosmochimica Acta, 77, 98–107, 2012.

Christl, M., Casacuberta, N., Vockenhuber, C., Elsässer, C., Bois, P. B. D., Herrmann, J., and Synal, H. A.: Reconstruction of the 236U input function for the Northeast Atlantic Ocean: Implications for 129I/236U and 236U/238U-based tracer ages, Journal of Geophysical Research: Oceans, 120, 7282–7299, 2015.

Christl, M., Gautschi, P., Maxeiner, S., Müller, A. M., Vockenhuber, C., and Synal, H. A.: 236U analyses with the ETH Zurich MILEA prototype system, Nuclear Instruments and Methods in Physics Research Section B: Beam Interactions with Materials and Atoms, 534, 61–71, 2023.

Dale, D., Christl, M., Vockenhuber, C., Macrander, A., Ólafsdóttir, S., Middag, R., and Casacuberta, N.: Tracing Ocean Circulation and Mixing From the Arctic to the Subpolar North Atlantic Using the 129I–236U Dual Tracer, Journal of Geophysical Research: Oceans, 129, e2024JC021 211, 2024.

de Steur, L.: Fram Strait cruise report, 24 August – 13 September 2020: cruise no. 2020709, 52, 2021.

de Steur, L.: Fram Strait cruise report, 31 July - 20 August 2021: cruise no. 2021709, 57, 2022.

de Steur, L., Hansen, E., Mauritzen, C., Beszczynska-Möller, A., and Fahrbach, E.: Impact of recirculation on the East Greenland Current in Fram Strait: Results from moored current meter measurements between 1997 and 2009, Deep Sea Research Part I: Oceanographic Research Papers, 92, 26–40, 2014.

Dey, D., Marsh, R., Drijfhout, S., Josey, S. A., Sinha, B., Grist, J., and Döös, K.: Formation of the Atlantic Meridional Overturning Circulation lower limb is critically dependent on Atlantic-Arctic mixing, Nature Communications 2024 15:1, 15, 1–10, 2024.

Dodd, P. A., Rabe, B., Hansen, E., Falck, E., MacKensen, A., Rohling, E., Stedmon, C., and Kristiansen, S.: The freshwater composition of the Fram Strait outflow derived from a decade of tracer measurements, Journal of Geophysical Research: Oceans, 117, 2012.

Dodd, P. A., Ask, A., Divine, D., Granskog, M. A., Keck, A., Kern, Y., Petit, T., Karpouzoglou, T., C. A., S., and de Steur, L.: CTD profiles from NPI cruise FS2020 to the Fram Strait including auxiliary sensors, Tech. rep., Norwegian Polar Institute, 2022a.

Dodd, P. A., Gonçalves-Araujo, R., Granskog, M. A., Jensen, A. D. B., Kern, Y., Lin, G., Hagen, S. Z., Haraguchi, L., Stedmon, C. A., and de Steur, L.: CTD profiles from NPI cruise FS2021 to the Fram Strait including auxiliary sensors, Tech. rep., Norwegian Polar Institute, 2022b.

Dörr, J. S., Mans, C. J., Årthun, M., Döös, K., Evans, D. G., and He, Y.: The Arctic overturning circulation: transformations, pathways and timescales, 2026.

https://doi.org/10.5194/egusphere-2026-2020
Preprint. Discussion started: 21 April 2026

Edmonds, H. N., Zhou, Z. Q., Raisbeck, G. M., Yiou, F., Kilius, L., and Edmond, J. M.: Distribution and behavior of anthropogenic 129I in water masses ventilating the North Atlantic Ocean, Journal of Geophysical Research: Oceans, 106, 6881–6894, 2001.

Ekwurzel, B., Schlosser, P., Mortlock, R. A., Fairbanks, R. G., and Swift, J. H.: River runoff, sea ice meltwater, and Pacific water distribution and mean residence times in the Arctic Ocean, Journal of Geophysical Research: Oceans, 106, 9075–9092, 2001.

Falck, E., Kattner, G., and Budéus, G.: Disappearance of Pacific Water in the northwestern Fram Strait, Geophysical Research Letters, 32, 1–4, 2005.

Falck, E., Jones, E. P., Kattner, G., and Budéus, G.: Fresh water in the northern East Greenland Current from 1982 through 2005, EPIC32008 Ocean Sciences Meeting, 2-7 March, Orlando, USA., 2008.

Fichot, C. G., Kaiser, K., Hooker, S. B., Amon, R. M., Babin, M., Bélanger, S., Walker, S. A., and Benner, R.: Pan-Arctic distributions of continental runoff in the Arctic Ocean, Scientific Reports 2013 3:1, 3, 1–6, 2013.

Gerke, L., Arck, Y., and Tanhua, T.: Temporal Variability of Ventilation in the Eurasian Arctic Ocean, Journal of Geophysical Research: Oceans, 129, e2023JC020 608, 2024.

Giles, K. A., Laxon, S. W., Ridout, A. L., Wingham, D. J., and Bacon, S.: Western Arctic Ocean freshwater storage increased by wind-driven spin-up of the Beaufort Gyre, Nature Geoscience 2012 5:3, 5, 194–197, 2012.

Granskog, M. A., Stedmon, C. A., Dodd, P. A., Amon, R. M., Pavlov, A. K., Steur, L. D., and Hansen, E.: Characteristics of colored dissolved organic matter (CDOM) in the Arctic outflow in the Fram Strait: Assessing the changes and fate of terrigenous CDOM in the Arctic Ocean, Journal of Geophysical Research: Oceans, 117, 12 021, 2012.

Greene, C. H., Pershing, A. J., Cronin, T. M., and Ceci, N.: Arctic climate change and its impacts on the ecology of the North Atlantic, Ecology, 89, S24–S38, 2008.

Guo, H., Koeve, W., Oschlies, A., He, Y.-C., Kemena, T. P., Gerke, L., and Kriest, I.: Dual-tracer constraints on the inverse Gaussian transit time distribution improve the estimation of water mass ages and their temporal trends in the tropical thermocline, Ocean Science, 21, 1167–1182, 2025.

Haine, T. W., Siddiqui, A. H., and Jiang, W.: Arctic freshwater impact on the Atlantic Meridional Overturning Circulation: status and prospects, Philosophical Transactions of the Royal Society A, 381, 2023.

Haine, T. W. N. and Hall, T. M.: A Generalized Transport Theory: Water-Mass Composition and Age, Journal of Physical Oceanography, 32, 1932–1946, 2002.

Haine, T. W. N., Griffies, S. M., Gebbie, G., and Jiang, W.: A Review of Green's Function Methods for Tracer Timescales and Pathways in Ocean Models, Journal of Advances in Modeling Earth Systems, 17, e2024MS004 637, 2025.

Hall, T. M. and Haine, T. W. N.: On Ocean Transport Diagnostics: The Idealized Age Tracer and the Age Spectrum, Journal of Physical Oceanography, 32, 1987–1991, 2002.

Hattermann, T., Isachsen, P. E., Appen, W. J. V., Albretsen, J., and Sundfjord, A.: Eddy-driven recirculation of Atlantic Water in Fram Strait, Geophysical Research Letters, 43, 3406–3414, 2016.

Heuzé, C., Huhn, O., Walter, M., Sukhikh, N., Karam, S., Körtke, W., Vredenborg, M., Bulsiewicz, K., Sültenfuß, J., Fang, Y. C., Mertens, C., Rabe, B., Tippenhauer, S., Allerholt, J., He, H., Kuhlmey, D., Kuznetsov, I., and Mallet, M.: A year of transient tracers (chlorofluorocarbon 12 and sulfur hexafluoride), noble gases (helium and neon), and tritium in the Arctic Ocean from the MOSAiC expedition (2019–2020), Earth System Science Data, 15, 5517–5534, 2023.

Hofmann, Z., von Appen, W. J., and Wekerle, C.: Seasonal and Mesoscale Variability of the Two Atlantic Water Recirculation Pathways in Fram Strait, Journal of Geophysical Research: Oceans, 126, e2020JC017 057, 2021.

https://doi.org/10.5194/egusphere-2026-2020
Preprint. Discussion started: 21 April 2026

Ingvaldsen, R. B., Assmann, K. M., Primicerio, R., Fossheim, M., Polyakov, I. V., and Dolgov, A. V.: Physical manifestations and ecological implications of Arctic Atlantification, Nature Reviews Earth & Environment 2021 2:12, 2, 874–889, 2021.

Jahn, A., Holland, M. M., and Kay, J. E.: Projections of an ice-free Arctic Ocean, Nature Reviews Earth & Environment 2024 5:3, 5, 164–176, 2024.

Jones, E. P., Anderson, L. G., and Swift, J. H.: Distribution of Atlantic and Pacific waters in the upper Arctic Ocean: Implications for circulation, Geophysical Research Letters, 25, 765–768, 1998.

Jones, E. P., Swift, J. H., Anderson, L. G., Lipizer, M., Civitarese, G., Falkner, K. K., Kattner, G., and McLaughlin, F.: Tracing Pacific water in the North Atlantic Ocean, Journal of Geophysical Research: Oceans, 108, 2003.

Jones, E. P., Anderson, L. G., Jutterström, S., and Swift, J. H.: Sources and distribution of fresh water in the East Greenland Current, Progress in Oceanography, 78, 37–44, 2008.

Kanzow, T. and Rohardt, G.: CTD raw data files from POLARSTERN cruise PS100, link to tar file, PANGAEA, 2017.

Karcher, M., Smith, J. N., Kauker, F., Gerdes, R., and Smethie, W. M.: Recent changes in Arctic Ocean circulation revealed by iodine-129 observations and modeling, Journal of Geophysical Research: Oceans, 117, 8007, 2012.

Karcher, M. J. and Oberhuber, J. M.: Pathways and modification of the upper and intermediate waters of the Arctic Ocean, Journal of Geophysical Research: Oceans, 107, 2–1, 2002.

Karpouzoglou, T., de Steur, L., Smedsrud, L. H., and Sumata, H.: Observed Changes in the Arctic Freshwater Outflow in Fram Strait, Journal of Geophysical Research: Oceans, 127, e2021JC018 122, 2022.

Karpouzoglou, T., Steur, L. D., Smedsrud, L. H., Karcher, M., and Sumata, H.: Three Forcing Mechanisms of Freshwater Transport in Fram Strait, Journal of Geophysical Research: Oceans, 129, e2024JC020 930, 2024.

Kim, Y.-H., Min, S.-K., Gillett, N. P., Notz, D., and Malinina, E.: Observationally-constrained projections of an ice-free Arctic even under a low emission scenario, Nature Communications 2023 14:1, 14, 1–8, 2023.

Kumamoto, Y., Hamajima, Y., Nishino, S., Inoue, M., Nagai, H., Matsuzaki, H., Yamagata, T., Murata, A., and Kikuchi, T.: Temporal changes in iodine-129 and radiocesium in the Canada Basin in the Arctic Ocean between 1993 and 2020, Polar Science, 41, 101 071, 2024.

Körtke, W., Walter, M., Huhn, O., Kanzow, T., and Rhein, M.: Decadal Changes in the Pathways of the Atlantic Water Core in the Arctic Ocean Inferred From Transient Tracers, Journal of Geophysical Research: Oceans, 129, e2024JC021 419, 2024.

Laukert, G., Frank, M., Hathorne, E. C., Krumpen, T., Rabe, B., Bauch, D., Werner, K., Peeken, I., and Kassens, H.: Pathways of Siberian Freshwater and Sea Ice in the Arctic Ocean Traced with Radiogenic Neodymium Isotopes and Rare Earth Elements, Polarforschung, 87, 3–13, 2017.

Leist, L. G., Castrillejo, M., Smith, J. N., Christl, M., Vockenhuber, C., Velo, A., Lherminier, P., and Casacuberta, N.: 129I and 236U distribution in the subpolar North Atlantic unravels water mass provenance in AR7W and A25 lines, Frontiers in Marine Science, 11, 1470 675, 2024.

Lin, G., Qiao, J., Dodd, P. A., Gonçalves-Araujo, R., Granskog, M. A., Steier, P., and Stedmon, C. A.: Tracing Atlantic water transit times in the Arctic Ocean: Coupling reprocessing-derived 236U and colored dissolved organic matter to distinguish different pathways, Earth and Planetary Science Letters, 622, 118 415, 2023a.

Lin, P., Pickart, R. S., Heorton, H., Tsamados, M., Itoh, M., and Kikuchi, T.: Recent state transition of the Arctic Ocean's Beaufort Gyre, Nature Geoscience, 16, 485–491, 2023b.

Lique, C., Treguier, A. M., Blanke, B., and Grima, N.: On the origins of water masses exported along both sides of Greenland: A Lagrangian model analysis, Journal of Geophysical Research: Oceans, 115, 2010.

https://doi.org/10.5194/egusphere-2026-2020
Preprint. Discussion started: 21 April 2026

Lique, C., Johnson, H. L., and Davis, P. E.: On the Interplay between the Circulation in the Surface and the Intermediate Layers of the Arctic Ocean, Journal of Physical Oceanography, 45, 1393–1409, 2015.

Manley, T. O.: Branching of Atlantic water within the Greenland-spitsbergen passage: An estimate of recirculation, Journal of Geophysical Research: Oceans, 100, 20,627–20,634, 1995.

Marnela, M., Rudels, B., Houssais, M.-N., Beszczynska-Möller, A., and Eriksson, P. B.: Recirculation in the Fram Strait and transports of water in and north of the Fram Strait derived from CTD data, Ocean Science, 9, 499–519, 2013.

Martin, T., Steele, M., and Zhang, J.: Seasonality and long-term trend of Arctic Ocean surface stress in a model, Journal of Geophysical Research: Oceans, 119, 1723–1738, 2014.

McAlister, J. A. and Orians, K. J.: Dissolved gallium in the Beaufort Sea of the Western Arctic Ocean: A GEOTRACES cruise in the International Polar Year, Marine Chemistry, 177, 101–109, 2015.

McPherson, R. A., Wekerle, C., and Kanzow, T.: Shifts of the Recirculation Pathways in Central Fram Strait Drive Atlantic Intermediate Water Variability on Northeast Greenland Shelf, Journal of Geophysical Research: Oceans, 128, e2023JC019 915, 2023.

Meredith, M. P., Sommerkorn, M., Cassotta, S., Derksen, C., Ekaykin, A. A., Hollowed, A. B., Kofinas, G., Mackintosh, A. N., Muelbert, M. M. C., Melbourne-Thomas, J., Ottersen, G., Pritchard, H. D., and Schuur, E. A. G.: Polar Regions. In: IPCC Special Report on the Ocean and Cryosphere in a Changing Climate, 2019.

Morison, J. H., Long, C. E., and Levine, M. D.: Internal wave dissipation under sea ice, Journal of Geophysical Research: Oceans, 90, 11 959–11 966, 1985.

Muilwijk, M., Hattermann, T., Martin, T., and Granskog, M. A.: Future sea ice weakening amplifies wind-driven trends in surface stress and Arctic Ocean spin-up, Nature Communications, 15, 1–15, 2024.

Ostlund, H. G. and Hut, G.: Arctic Ocean water mass balance from isotope data, Journal of Geophysical Research: Oceans, 89, 6373–6381, 1984.

Paffrath, R., Laukert, G., Bauch, D., van der Loeff, M. R., and Pahnke, K.: Separating individual contributions of major Siberian rivers in the Transpolar Drift of the Arctic Ocean, Scientific Reports 2021 11:1, 11, 8216–, 2021.

Pasqualini, A., Schlosser, P., Newton, R., Smethie, W. M., and Friedrich, R.: A Multi-Decade Tracer Study of the Circulation and Spreading Rates of Atlantic Water in the Arctic Ocean, Journal of Geophysical Research: Oceans, 129, e2023JC020 738, 2024.

Payne, A., Wefing, A. M., Christl, M., Vockenhuber, C., Williams, W., Smith, J. N., and Casacuberta, N.: Circulation Timescales and Pathways of Atlantic Water in the Canada Basin: Insights From Transient Tracers 129I and 236U, Journal of Geophysical Research: Oceans, 129, e2023JC020 813, 2024.

Peacock, S. and Maltrud, M.: Transit-Time Distributions in a Global Ocean Model, Journal of Physical Oceanography, 36, 474–495, 2006.

Pemberton, P., Nilsson, J., and Meier, H. E.: Arctic ocean freshwater composition, pathways and transformations from a passive tracer simulation, Tellus, Series A: Dynamic Meteorology and Oceanography, 66, 2014.

Planat, N., Tremblay, L. B., Dufour, C. O., and Straub, D.: Seasonal and Decadal Geostrophic Pathways of Pacific and Atlantic Waters in the Arctic Amerasian Basin From Observations, Journal of Geophysical Research: Oceans, 130, e2024JC021 560, 2025.

Polyakov, I. V., Alkire, M. B., Bluhm, B. A., Brown, K. A., Carmack, E. C., Chierici, M., Danielson, S. L., Ellingsen, I., Ershova, E. A., Gårdfeldt, K., Ingvaldsen, R. B., Pnyushkov, A. V., Slagstad, D., and Wassmann, P.: Borealization of the Arctic Ocean in Response to Anomalous Advection From Sub-Arctic Seas, Frontiers in Marine Science, 7, 516 272, 2020a.

https://doi.org/10.5194/egusphere-2026-2020
Preprint. Discussion started: 21 April 2026

Polyakov, I. V., Rippeth, T. P., Fer, I., Baumann, T. M., Carmack, E. C., Ivanov, V. V., Janout, M., Padman, L., Pnyushkov, A. V., and Rember, R.: Intensification of Near-Surface Currents and Shear in the Eastern Arctic Ocean, Geophysical Research Letters, 47, e2020GL089 469, 2020b.

Polyakov, I. V., Ingvaldsen, R. B., Pnyushkov, A. V., Bhatt, U. S., Francis, J. A., Janout, M., Kwok, R., and Øystein Skagseth: Fluctuating Atlantic inflows modulate Arctic atlantification, Science (New York, N.Y.), 381, 972–979, 2023.

Polyakov, I. V., Pnyushkov, A. V., Carmack, E. C., Charette, M., Cho, K.-H., Dykstra, S., Haapala, J., Jung, J., Kipp, L., and Yang, E. J.: Role of sea ice, stratification, and near-inertial oscillations in shaping the upper Siberian Arctic Ocean currents, 2025a.

Polyakov, I. V., Pnyushkov, A. V., Charette, M., Cho, K.-H., Jung, J., Kipp, L., Muilwijk, M., Whitmore, L., Yang, E. J., and Yoo, J.: Atlantification advances into the Amerasian Basin of the Arctic Ocean, Science Advances, 11, 7580, 2025b.

Popova, E. E., Yool, A., Aksenov, Y., and Coward, A. C.: Role of advection in Arctic Ocean lower trophic dynamics: A modeling perspective, Journal of Geophysical Research: Oceans, 118, 1571–1586, 2013.

Previdi, M., Smith, K. L., and Polvani, L. M.: Arctic amplification of climate change: a review of underlying mechanisms, Environmental Research Letters, 16, 093 003, 2021.

Proshutinsky, A., Krishfield, R., Toole, J. M., Timmermans, M. L., Williams, W., Zimmermann, S., Yamamoto-Kawai, M., Armitage, T. W., Dukhovskoy, D., Golubeva, E., Manucharyan, G. E., Platov, G., Watanabe, E., Kikuchi, T., Nishino, S., Itoh, M., Kang, S. H., Cho, K. H., Tateyama, K., and Zhao, J.: Analysis of the Beaufort Gyre Freshwater Content in 2003–2018, Journal of Geophysical Research: Oceans, 124, 9658–9689, 2019.

Pérez-Tribouillier, H., Jaccard, S. L., Blaser, P., Christl, M., Creac'h, L., Hölemann, J., Scheiwiller, M., Vockenhuber, C., Wefing, A. M., and Casacuberta, N.: The Role of the St. Anna Trough in Atlantic Water Transport Into the Arctic Ocean: A Novel Radiogenic Isotope Assessment Using Iodine, Uranium, and Neodymium, Journal of Geophysical Research: Oceans, 130, e2024JC022 050, 2025.

Quadfasel, D., Gascard, J.-C., and Koltermann, K.-P.: Large-scale oceanography in Fram Strait during the 1984 Marginal Ice Zone Experiment, Journal of Geophysical Research: Oceans, 92, 6719–6728, 1987.

Rabe, B., Dodd, P. A., Hansen, E., Falck, E., Schauer, U., MacKensen, A., Beszczynska-Möller, A., Kattner, G., Rohling, E. J., and Cox, K.: Liquid export of Arctic freshwater components through the Fram Strait 1998–2011, Ocean Science, 9, 91–109, 2013.

Raimondi, L., Wefing, A. M., and Casacuberta, N.: Anthropogenic Carbon in the Arctic Ocean: Perspectives From Different Transient Tracers, Journal of Geophysical Research: Oceans, 129, e2023JC019 999, 2024.

Raisbeck, G. M., Yiou, F., Zhou, Z. Q., and Kilius, L. R.: 129I from nuclear fuel reprocessing facilities at Sellafield (U.K.) and La Hague (France); potential as an oceanographie tracer, Journal of Marine Systems, 6, 561–570, 1995.

Rudels, B.: Arctic Ocean Circulation, Encyclopedia of Ocean Sciences, pp. 211–225, 2009.

Rudels, B.: The Physical Oceanography of the Arctic Mediterranean Sea: Explorations, Observations, Interpretations, Elsevier, ISBN 9780128169308, 2021.

Rudels, B. and Carmack, E.: Arctic ocean water mass structure and circulation, Oceanography, 35, 52–65, 2022.

Rudels, B., Jones, E. P., Anderson, L. G., Kattner, G., Rudels, B., Jones, E. P., Anderson, L. G., and Kattner, G.: On the intermediate depth waters of the Arctic Ocean, GMS, 85, 33–46, 1994.

Rudels, B., Meyer, R., Fahrbach, E., Ivanov, V. V., Østerhus, S., Quadfasel, D., Schauer, U., Tverberg, V., and Woodgate, R. A.: Water mass distribution in Fram Strait and over the Yermak Plateau in summer 1997, Annales Geophysicae, 18, 687–705, 2000.

Rudels, B., Fahrbach, E., Meincke, J., Budéus, G., and Eriksson, P.: The East Greenland Current and its contribution to the Denmark Strait overflow, ICES Journal of Marine Science, 59, 1133–1154, 2002.

https://doi.org/10.5194/egusphere-2026-2020
Preprint. Discussion started: 21 April 2026

Rudels, B., Korhonen, M., Schauer, U., Pisarev, S., Rabe, B., and Wisotzki, A.: Circulation and transformation of Atlantic water in the Eurasian Basin and the contribution of the Fram Strait inflow branch to the Arctic Ocean heat budget, Progress in Oceanography, 132, 128–152, 2015.

Sakaguchi, A., Kawai, K., Steier, P., Quinto, F., Mino, K., Tomita, J., Hoshi, M., Whitehead, N., and Yamamoto, M.: First results on 236U levels in global fallout, Science of The Total Environment, 407, 4238–4242, 2009.

Schauer, U., Fahrbach, E., Osterhus, S., and Rohardt, G.: Arctic warming through the Fram Strait: Oceanic heat transport from 3 years of measurements, Journal of Geophysical Research: Oceans, 109, 2004.

Scheiwiller, M.: I-129 and U-236 data from the Fram Strait in 2020 and 2021, https://doi.org/10.5281/ZENODO.19387002, 2026.

Shu, Q., Wang, Q., Årthun, M., Wang, S., Song, Z., Zhang, M., and Qiao, F.: Arctic Ocean Amplification in a warming climate in CMIP6 models, Science Advances, 8, 9755, 2022.

Smedsrud, L. H., Muilwijk, M., Brakstad, A., Madonna, E., Lauvset, S. K., Spensberger, C., Born, A., Eldevik, T., Drange, H., Jeansson, E., Li, C., Olsen, A., Øystein Skagseth, Slater, D. A., Straneo, F., Våge, K., and Årthun, M.: Nordic Seas Heat Loss, Atlantic Inflow, and Arctic Sea Ice Cover Over the Last Century, Reviews of Geophysics, 60, e2020RG000 725, 2022.

Smith, J. N., Ellis, K. M., and Boyd, T.: Circulation features in the central Arctic Ocean revealed by nuclear fuel reprocessing tracers from Scientific Ice Expeditions 1995 and 1996, Journal of Geophysical Research: Oceans, 104, 29 663–29 677, 1999.

Smith, J. N., McLaughlin, F. A., Smethie, W. M., Moran, S. B., and Lepore, K.: Iodine-129, 137Cs, and CFC-11 tracer transit time distributions in the Arctic Ocean, Journal of Geophysical Research: Oceans, 116, 4024, 2011.

Smith, J. N., Karcher, M., Casacuberta, N., Williams, W. J., Kenna, T., and Smethie, W. M.: A Changing Arctic Ocean: How Measured and Modeled 129I Distributions Indicate Fundamental Shifts in Circulation Between 1994 and 2015, Journal of Geophysical Research: Oceans, 126, e2020JC016 740, 2021.

Smith, J. N., Smethie, W. M., and Casacuberta, N.: Synoptic 129I and CFC–SF6 Transit Time Distribution (TTD) Sections Across the Central Arctic Ocean From the 2015 GEOTRACES Cruises, Journal of Geophysical Research: Oceans, 127, e2021JC018 120, 2022.

Snyder, G., Aldahan, A., and Possnert, G.: Global distribution and long-term fate of anthropogenic 129I in marine and surface water reservoirs, Geochemistry, Geophysics, Geosystems, 11, 2010.

Steele, M., Morison, J., Ermold, W., Rigor, I., Ortmeyer, M., and Shimada, K.: Circulation of summer Pacific halocline water in the Arctic Ocean, Journal of Geophysical Research: Oceans, 109, 2004.

Stöven, T., Tanhua, T., Hoppema, M., and Appen, W. J. V.: Transient tracer distributions in the Fram Strait in 2012 and inferred anthropogenic carbon content and transport, Ocean Science, 12, 319–333, 2016.

Tesi, T., Muschitiello, F., Mollenhauer, G., Miserocchi, S., Langone, L., Ceccarelli, C., Panieri, G., Chiggiato, J., Nogarotto, A., Hefter, J., Ingrosso, G., Giglio, F., Giordano, P., and Capotondi, L.: Rapid Atlantification along the Fram Strait at the beginning of the 20th century, Science Advances, 7, 2946, 2021.

Timmermans, M. L. and Marshall, J.: Understanding Arctic Ocean Circulation: A Review of Ocean Dynamics in a Changing Climate, Journal of Geophysical Research: Oceans, 125, e2018JC014 378, 2020.

Timmermans, M. L. and Toole, J. M.: The Arctic Ocean's Beaufort Gyre, Annual Review of Marine Science, 15, 223–248, 2023.

Vockenhuber, C., Casacuberta, N., Christl, M., and Synal, H. A.: Accelerator Mass Spectrometry of 129I towards its lower limits, Nuclear Instruments and Methods in Physics Research Section B: Beam Interactions with Materials and Atoms, 361, 445–449, 2015.

https://doi.org/10.5194/egusphere-2026-2020
Preprint. Discussion started: 21 April 2026

Wang, Q., Wekerle, C., Wang, X., Danilov, S., Koldunov, N., Sein, D., Sidorenko, D., von Appen, W. J., and Jung, T.: Intensification of the Atlantic Water Supply to the Arctic Ocean Through Fram Strait Induced by Arctic Sea Ice Decline, Geophysical Research Letters, 47, e2019GL086 682, 2020.

Wang, Q., Shu, Q., and Wang, F.: Recent emergence of Arctic atlantification dominated by climate warming, Science Advances, 10, 2024.

Wang, Y., Bi, H., and Liang, Y.: A Satellite-Observed Substantial Decrease in Multiyear Ice Area Export through the Fram Strait over the Last Decade, Remote Sensing, 14, 2022.

Waugh, D. W., Vollmer, M. K., Weiss, R. F., Haine, T. W. N., and Hall, T. M.: Transit time distributions in Lake Issyk-Kul, Geophysical Research Letters, 29, 84–1, 2002.

Waugh, D. W., Hall, T. M., and Haine, T. W. N.: Relationships among tracer ages, Journal of Geophysical Research: Oceans, 108, 2003.

Waugh, D. W., Haine, T. W., and Hall, T. M.: Transport times and anthropogenic carbon in the subpolar North Atlantic Ocean, Deep Sea Research Part I: Oceanographic Research Papers, 51, 1475–1491, 2004.

Wefing, A.-M., Christl, M., Vockenhuber, C., van der Loeff, M. R., and Casacuberta, N.: Tracing Atlantic Waters Using 129I and 236U in the Fram Strait in 2016, Journal of Geophysical Research: Oceans, 124, 882–896, 2019.

Wefing, A.-M., Casacuberta, N., Christl, M., Gruber, N., and Smith, J. N.: Circulation timescales of Atlantic Water in the Arctic Ocean determined from anthropogenic radionuclides, Ocean Science, 17, 111–129, 2021.

Wefing, A.-M., Casacuberta, N., Christl, M., and Dodd, P. A.: Water mass composition in Fram Strait determined from the combination of 129I and 236U: Changes between 2016, 2018, and 2019, Frontiers in Marine Science, p. 1598, 2022.

Wefing, A.-M., Payne, A., Scheiwiller, M., Vockenhuber, C., Christl, M., Tanhua, T., and Casacuberta, N.: Changes in Atlantic Water circulation in the central Arctic Ocean between 2011 and 2021 inferred from tracer observations, 2025.

Weijer, W., Haine, T. W. N., Siddiqui, A. H., Cheng, W., Veneziani, M., and Kurtakoti, P.: INTERACTIONS BETWEEN THE ARCTIC MEDITERRANEAN AND THE ATLANTIC MERIDIONAL OVERTURNING CIRCULATION: A REVIEW, Oceanography, 35, 118–127, 2022.

Wekerle, C., Wang, Q., von Appen, W. J., Danilov, S., Schourup-Kristensen, V., and Jung, T.: Eddy-Resolving Simulation of the Atlantic Water Circulation in the Fram Strait With Focus on the Seasonal Cycle, Journal of Geophysical Research: Oceans, 122, 8385–8405, 2017.

Whitmore, L. M., Pasqualini, A., Newton, R., and Shiller, A. M.: Gallium: A New Tracer of Pacific Water in the Arctic Ocean, Journal of Geophysical Research: Oceans, 125, e2019JC015 842, 2020.

Wilson, C., Aksenov, Y., Rynders, S., Kelly, S. J., Krumpen, T., and Coward, A. C.: Significant variability of structure and predictability of Arctic Ocean surface pathways affects basin-wide connectivity, Communications Earth & Environment 2021 2:1, 2, 164–, 2021.

Woodgate, R.: Arctic Ocean circulation: Going around at the top of the world, psc.apl.washington.edu, 2013.

Woodgate, R. A., Aagaard, K., Muench, R. D., Gunn, J., Björk, G., Rudels, B., Roach, A. T., and Schauer, U.: The Arctic Ocean Boundary Current along the Eurasian slope and the adjacent Lomonosov Ridge: Water mass properties, transports and transformations from moored instruments, Deep Sea Research Part I: Oceanographic Research Papers, 48, 1757–1792, 2001.

Zhang, R. and Thomas, M.: Horizontal circulation across density surfaces contributes substantially to the long-term mean northern Atlantic Meridional Overturning Circulation, Communications Earth & Environment 2021 2:1, 2, 1–12, 2021.

Årthun, M., Brakstad, A., Dörr, J., Johnson, H. L., Mans, C., Semper, S., and Våge, K.: Atlantification drives recent strengthening of the Arctic overturning circulation, Science Advances, 11, 1794, 2026.